Empirical Model, Capacity Recovery-Identification Correction and Machine Learning Co-Driven Li-ion Battery Remaining Useful Life Prediction

Zhigang Lv, Zhiwen Chen, Peng Wang, Chu Wang, Ruohai Di, Xiaoyan Li, Hui Gao

Title: Empirical Model, Capacity Recovery-Identification Correction and Machine Learning Co-Driven Li-ion Battery Remaining Useful Life Prediction

Zhigang Lv[a,b], Zhiwen Chen[b,*], Peng Wang[b], Chu Wang[b], Ruohai Di[b], Xiaoyan Li[b], Hui Gao[b]
a School of Mechatronic Engineering, Xi'an Technological University, China
b School of Electronics and Information Engineering, Xi'an Technological University, China
*Corresponding author: Zhiwen Chen (E-mail address: 1002129839@qq.com)

Abstract: Li-ion battery is the most important energy storage and conversion device. RUL prediction, as an important part of the battery health management system, provides important information for specifying energy control strategies and preventing Li-ion battery failure. In this paper, Empirical Model, Capacity Recovery-Identification Correction and Machine Learning co-driven method was proposed to address the inaccurate and unreliable RUL predictions of Li-ion batteries caused by difference data and non-stationary trends. Firstly, on the basis of using only the historical data of the target Li-ion battery, the acknowledged bi-exponential degradation model was used to generate the guidance sequence, which guides the output of the machine learning model and avoids the unsatisfactory prediction effect caused by difference data. Secondly, the recoverable capacity present during the capacity degradation process was analyzed and identified, and overly aggressive or conservative predictions caused by non-stationary trends were avoided by correcting the historical recoverable capacity. Finally, experiment results on publicly available datasets show that the method proposed in this paper can effectively improve the accuracy of the prediction using historical data, with MAPE of the degradation trend prediction being only 3.79%, and the average RA of RUL prediction for different failure thresholds remaining at the level of 90%.
Keywords: Li-ion Battery; RUL prediction; Empirical Model; Recovery-Identification Correction.

1 Introduction

Li-ion batteries, a new green renewable energy storage and conversion device, have broad applications. Li-ion batteries can not only effectively store clean energy such as wind and solar, but also provide power to new energy vehicles. This is an important way to achieve sustainable development and green low-carbon transformation [1]. As Li-ion batteries are being used in more and more devices, safety is being taken more and more seriously. Researchers have found that there is irreversible aging of Li-ion batteries [2]. If the aging Li-ion batteries are not repaired and replaced in time, leakage, combustion and explosion may occur, resulting in huge safety risks and economic losses. Therefore, the battery health management system was developed to ensure the safe and stable operation of Li-ion batteries by monitoring the charging and discharging process, estimating the health status, and predicting the aging failure [3].

In a battery health management system, the remaining useful life (RUL) of a Li-ion battery plays a crucial role in condition assessment and maintenance decisions for Li-ion batteries. RUL is the length of time that a battery can operate normally before it needs to be repaired or replaced. Some researchers analyze the degradation process of Li-ion batteries and extract health features [4], which are used as inputs to predict SOH [5]. Their work has made an important contribution to the analysis of the degradation mechanism of Li-ion batteries, but these methods can only obtain the SOH state at the current moment and cannot predict the future SOH trend, so it is difficult to predict the RUL of Li-ion batteries in use in practical application. More and more researchers obtain the RUL by first predicting the trend of capacity or SOH from the historical data of the battery, and then calculating the difference between the time in the future when the capacity or SOH drops to the failure threshold and the current time [6].

There have been a large number of researches on RUL prediction. The mainstream approaches are categorized into empirical model, data-driven model and hybrid model [7][8]. Empirical model is an approach based on empirical formulas and historical data. It establishes a mathematical formula to fit the degradation process by summarizing the degradation data of many full life cycles. For Li-ion batteries,

polynomial or exponential functions are often used to establish the capacity or SOH degradation process [9]. Data-driven model is an approach based on big data analysis and pattern recognition. Data driven methods do not rely on physical mechanisms and a priori knowledge, so can be used for different types of objects. However, the models are less interpretable, which is a criticism of data driven methods. There are lots of data driven methods that have been developed, such as support vector machine (SVM) [10], relevance vector machine (RVM) [11], Probabilistic Neural Network (PNN) [12], Dynamic Bayesian Networks (DBN) [13], and Wiener Process (WP) [14], etc. Hybrid model is an approach based on two and more models. It combines multiple models to avoid the drawbacks of a single model. Zhiqiang Lyu et al [15]. constructed a hybrid model containing RVM, LSTM, and FNN, which combined the advantages of each network to achieve RUL prediction with higher accuracy. Hybrid models can combine the advantages of multiple models while circumventing the disadvantages [16]. However, in order to achieve this function, more research and optimization of model fusion and coordination are needed.

1.1 Problems in RUL Prediction of Li-ion batteries

With the continuous research on RUL prediction of Li-ion batteries, researchers have found that it is difficult to accurately predict the future state of Li-ion batteries. This is manifested in the following areas:

(1) Li-ion battery is mainly composed of positive electrode, negative electrode, electrolyte and diaphragm. The current production process can't guarantee that the composition of the two batteries' materials is identical, resulting in a difference in the performance of the same type of batteries [17]. This difference in performance between individuals makes it difficult to construct a generic model of the same type of batteries from data on individual cells. Therefore, in order to construct an accurate model of the target Li-ion battery, it is often necessary to use the historical operating data of this Li-ion battery [18].

(2) The operating data of a single Li-ion battery increases with the duration of use. Only early operating data is available in the early stages of Li-ion battery commissioning. This is not enough data in relation to the full life cycle of a lithium-ion battery. The distribution characteristics of early operational data are different from those of full life cycle data. Models for predicting the full lifecycle state of a lithium-ion battery built from this data cannot accurately describe the future performance degradation process of this Li-ion battery, resulting in a low prediction reliability [19].

(3) The capacity degradation process of Li-ion batteries is characterized by non-fixed-length periodic plunges and recoveries, forming a non-monotonically decreasing degradation trend. Such non-monotonically decreasing data makes it easy for models trained on historical data to focus on data with large fluctuations at the end of the historical data, and cannot learn the overall data trend well, which can easily lead to overly aggressive or conservative predictions [20].

1.2 Relevant Researches to Address These Problems

A number of researchers have already been in touch with these issues and are at the beginning of their research in this direction. Chou JH et al. [21] obtained good RUL prediction based on transfer learning. Zhang Q et al. [22] used transfer learning to solve the modeling challenge with limited data. Large amounts of similar data are required for transfer learning. However, there is relatively little degradation data available for the same type of Li-ion battery, and the degradation trends of these data are different. This means that they can play little part in referencing. Therefore, more and more researchers expect to solve the challenge of RUL prediction by using the historical data of the Li-ion battery itself.

In the prediction problem, the difference data mainly means that the distribution range of the historical data does not match the distribution range of the future data, e.g. the historical data is distributed in [0.8, 1] and the future data is distributed in [0.4, 0.8]. Prediction models trained on difference data are extremely accurate when trained and validated on historical data, but their accuracy drops dramatically when tested on future data. It is highly likely that the model output will not be able to span the historical data distribution or diverge significantly. There have been researchers who have constructed a model suitable for a specific purpose by informing the model of a priori/expert knowledge in a specific form and letting the model follow the guidance of the knowledge to complete the training/learning. For example, Wang C et al. [23] used a statistical method to first analyze the degradation trend of the fuel cell and input this degradation trend as a guidance sequence into the data-driven method to achieve the prediction, which to some extent overcame the drawbacks of the difference data.

In the field of fault diagnosis/prediction, the phenomenon of experiencing a period of failure and

then returning to normal and occurring periodically is generally referred to as recoverable/reversible failure. In Li-ion batteries, many researchers do not call this type of phenomenon by the same name, such as capacity recovery, capacity restoration, capacity mutation and so on [2]. In this paper, this phenomenon is referred to as capacity recovery, and the Li-ion battery capacity data segment exhibiting this phenomenon is referred to as recoverable capacity. For recoverable/reversible faults, academics are divided into two directions of solution: one is to filter out recoverable faults as anomalous data and not to be used for training the model, and the other is to include recoverable faults as one of the categories of faults that need to be diagnosed or as part of those that need to be predicted. For example, Hao L et al. [24] decomposed the capacity sequence of a battery into a degradation trend sequence and a capacity recovery fluctuation sequence by CEEMD and modelled them separately for prediction. Yue M et al. [25] designed a CNN-based recursive multistep performance prediction method that detects the seasonality of the data in order to correct the prediction results by considering intermittent performance recovery.

In this paper, we address this problem of unsatisfactory data presented during the degradation of Li-ion batteries, expecting to predict the degradation trend and calculate the RUL under the condition of differential data formed by the inconsistency of the distribution characteristics of the historical data and the full life cycle data and under the condition of non-stationary trend caused by non-fixed-length periodic plunges and recoveries. The main contributions of this paper are as follows:

(1) Predict the future SOH and calculate RUL on the basis of historical data.

(2) Empirical formulae and data-driven are used to jointly complete the RUL predictions and address poor predictions caused by different data.

(3) Identify the recoverable capacity present during degradation and improve the prediction reliability of the model by correcting this data.

This study is intended to help predict the RUL for Li-ion battery in a more accurate way. To provide a reference methodology for battery health management systems, thereby helping to extend battery life, reduce maintenance costs and improve system reliability.

2 Methodology

2.1 Time Series Prediction Model

Definition of time series: an ordered array composed of sequential times of occurrence. Any time series can be considered to consist of a trend series, a periodic series and a random noise series [26]. The formula is expressed as follows:

$$X_t = T_t + S_t + R_t, t = 1, 2, 3, \cdots, n \quad (1)$$

where X_t denotes the time series, T_t denotes the trend term, S_t denotes the period term, R_t denotes the noise, and t denotes the time.

Temporal network is a model for predicting the future trend direction by studying and analyzing the time series data pattern and the deep feature information hidden in the time series data. In general, a single temporal network can only predict one outcome, and the predicted outcome is highly uncertain due to the stochastic nature of the model's initial parameters. The integrated temporal network can predict multiple results through multiple temporal networks, and then weighting multiple results can obtain the prediction results with a higher degree of confidence. This method can improve the stability and reliability of the model. The integrated temporal network structure used in this paper is shown in Fig.1. The integrated temporal network contains *n* temporal networks, and the data of historical stages are provided as training sets to *n* temporal networks for training respectively. The well-trained temporal network uses the last part of the historical data to predict the future data, and then treats the predicted future data as historical data and iteratively feeds it into the model to produce long term future predictions.

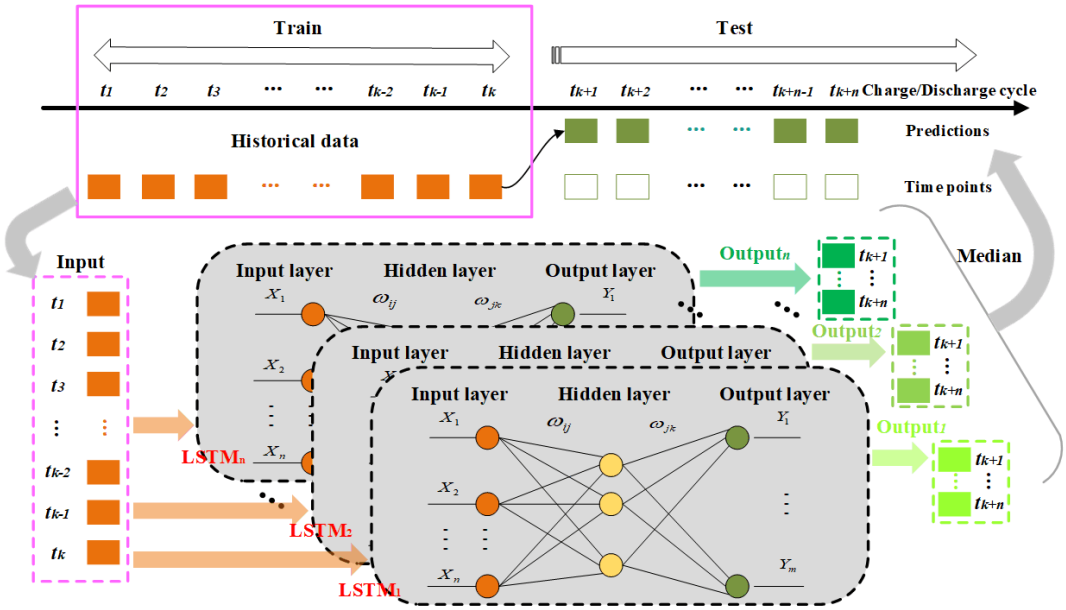

Fig. 1. The integrated temporal network structure

Long Short-Term Memory Network (LSTM) is an improved Recurrent Neural Network (RNN). In theory, RNN can handle arbitrarily long time series. However, there are problems with gradient vanishing and explosion during model training. When the weight matrix within the RNN model is updated by the backpropagation algorithm, the propagation of the gradient between the network weight matrices is also propagated along with the temporal dimension of the sequence. When the time series exceeds a certain length, there is a situation where the gradient becomes larger (or smaller) as the length of the series increases, and then there is a gradient explosion (disappearance of the gradient), which results in the model not being able to output the desired results. This makes it difficult to train RNN for long time sequences. LSTM incorporates three gate control units into its internal structure, which to some extent solves the problem of gradient vanishing and gradient explosion [27]. In this paper, LSTM is selected as the base network for the integrated temporal network.

2.2 A Framework for Prediction of Li-ion Battery Incorporating Priori Knowledge

2.2.1 Empirical Model of Li-ion Battery Degradation

During charging, lithium ions move from the positive electrode (usually lithium metal oxide) through the electrolyte to the negative electrode (usually graphite). During discharge, lithium ions are then released from the negative electrode and returned through the electrolyte to the lithium metal oxide lattice at the positive electrode. This process is carried out by means of ionic conduction in the electrolyte [2].

Over time, the electrolyte in the battery will also deteriorate. The electrolyte may decompose, dissolve, or react with the electrodes to form a solid electrolyte interface layer (SEI) or other degradation products from processes within the battery. These degradation products increase the internal resistance of the electrolyte and limit the migration rate of lithium ions, resulting in degraded battery performance, including capacity loss, increased internal resistance and reduced safety. SEI usually consists of electrolyte degradation products, including organic compounds and inorganic salts. SEI inhibits the migration of lithium ions and increases the internal impedance of the battery, leading to capacity loss and reduced electrochemical stability of the electrode materials [28].

Li-ion batteries accumulate dead lithium and thicken the SEI during charging. The external manifestation of SEI thickening is that the current across the SEI increases, while the interpolar current remains unchanged, the transmembrane current decreases, which brings about the degradation of the capacity and shortens the time to "full charge". Li-ion batteries activate the release of some of the dead lithium and thin the SEI during discharge. The external manifestation of SEI thinning is that the current across the SEI decreases, the current between the poles remains unchanged, the transmembrane current increases, which brings about the recovery of the capacity of the battery, and the "discharged" time becomes longer.

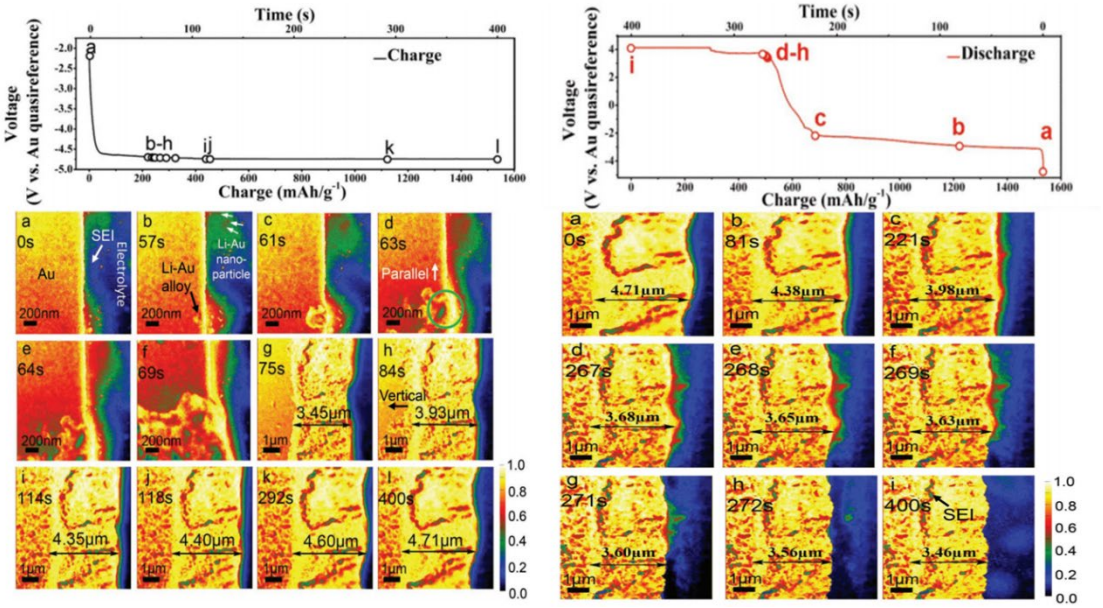

Fig. 2. The state of SEI during charging and discharging of Li-ion battery [28]

In summary, during the charge/discharge cycle of Li-ion batteries, the battery capacity shows the overall degradation of the "diffusion" process with time, and in the short cycle, it will show the "jump" process of capacity recovery, so the jump-diffusion model to characterize the degradation process of Li-ion batteries is Therefore, the jump-diffusion model is reasonable to characterize the decay process of Li-ion battery. However, during the modelling process, the authors found that time series data with random jumps had a negative effect on model predictions, much less so than the use of smooth curves incorporated into the model, so it was considered acceptable to reasonably ignore the jumping process during the modelling process. In this paper, the accepted bi-exponential model [8] was selected as the empirical model for the joint construction of the prediction model of Li-ion battery.

$$Capacity_t = A_1 e^{B_1 t + C_1} + A_2 e^{B_2 t + C_2} + D \tag{2}$$

where $Capacity_t$ represents the capacity corresponding to the number of charge/discharge cycles t and $A_1, B_1, C_1, A_2, B_2, C_2, D$ represents the parameter.

2.2.2 Prediction Methods based on Prior Knowledge Guidance Sequence

Firstly, the bi-exponential model of the target Li-ion battery was estimated based on historical data, from which the capacity degradation rate was extracted and grafted to the real test point to generate the guidance sequence. Secondly, multiple LSTMs were trained using historical data and the prediction of the model was implemented using guidance sequences as input. Finally, the median of the predictions from multiple LSTMs was calculated to obtain the SOH degradation trend, thus estimating the RUL. The schematic of the prediction strategy based on the guidance sequence is shown in Fig. 3.

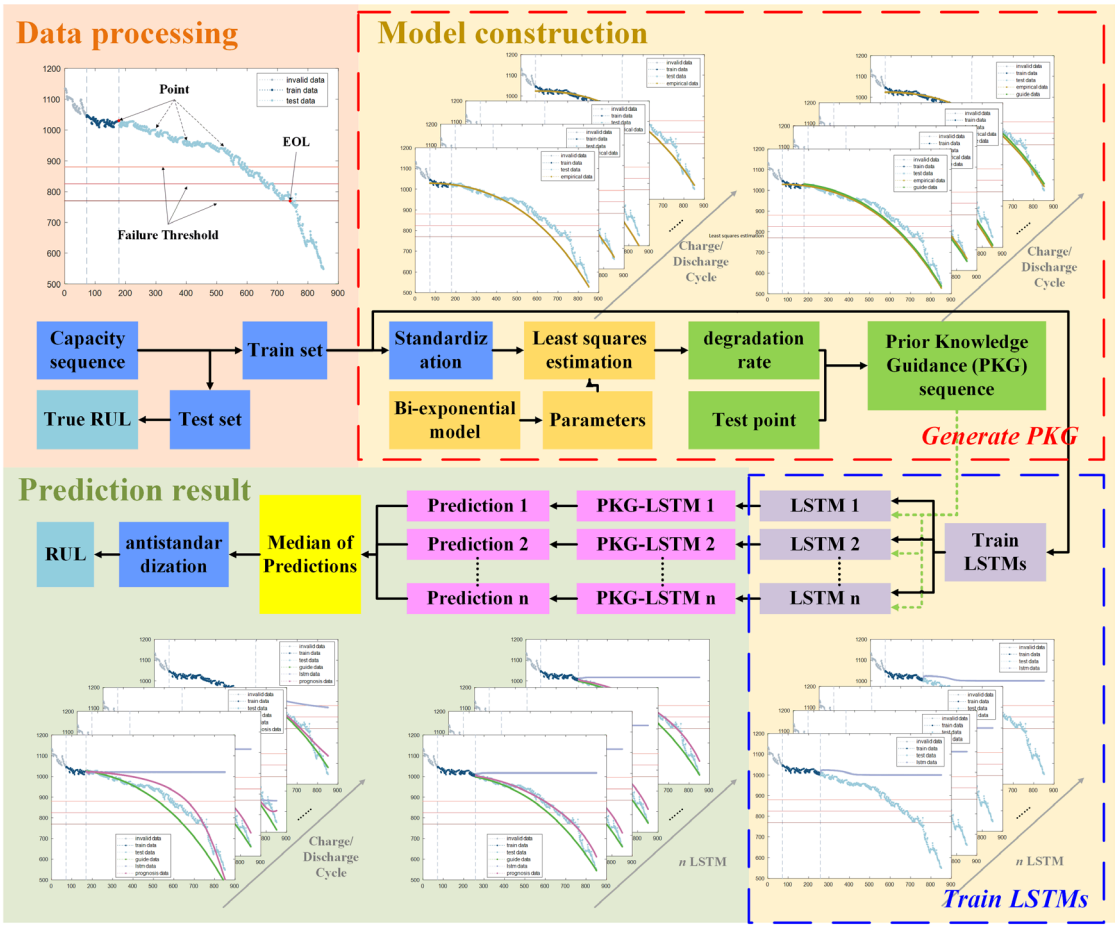

Fig. 3. Prediction strategy based on guidance sequence

(1) Generate Prior Knowledge Guidance Sequence

The guidance sequence generation process is shown in the red dashed box in Fig. 3. Historical data from the target Li-ion battery was used to estimate the initial parameters of the bi-exponential model. It is worth noting that using the same type of Li-ion battery data can obtain the initial parameters faster and better. Of course, the parameters of the bi-exponential model must be rescaled to the historical data of the target Li-ion battery. The degradation rate for the real test set was extracted from this. Finally, it was grafted onto the last data of the training set to form the Prior Knowledge Guidance (PKG) sequence.

(2) Train Long Short-Term Memory Networks

In the training phase of the LSTM, a rolling loop was used in which capacity information of a fixed time length was selected as input and the capacity at the next time will be predicted in this way. Any well-trained LSTM can be considered to perform well on the training set, but there was often a significant difference in performance on the test set. Training multiple LSTMs generates multiple prediction models, such as *LSTM 1*, *LSTM 2*, ..., *LSTM n* as shown in the blue dashed box in Fig. 3. This behavior facilitates the provision of diverse prediction results, which will further characterize the uncertainty of the model and improve the stability of the final results [29].

(3) Predict Degradation Trends

The multi-step prediction was achieved by iteratively using well-trained LSTMs for the single-step prediction. Specifically, in order to break the interval of historical values and reduce the accumulated single-step prediction error, the PKG was used as a model input rather than the previous step prediction. A series of LSTMs (PKG-LSTM 1, PKG -LSTM 2, ..., PKG -LSTM n) incorporating prior knowledge were formed by multiple well-trained LSTMs. These PKG -LSTM models will give *n* different predictions of Li-ion battery capacity degradation, and the trend consisting of the median of these predictions will be used as the final predicted battery capacity degradation trend.

(4) Calculate RUL

The RUL ($\widehat{RUL}_{t_i}$) at the time of t_i was calculated according to the following formula:

$$\widehat{RUL}_{t_i} = EOL_{t_i} - t_i \tag{3}$$

Where, EOL_{t_i} is the time when the estimated degradation trend first reaches the failure threshold (FT).

2.3 A Framework for Prediction by State Recognition and Data-driven

2.3.1 Recoverable Capacity Identification

It is necessary to identify short term anomalies in the process of capacity degradation, which distinguish it from the inherent trend of capacity degradation. For example, decline and recovery phases of capacity degradation. In particular, it is necessary to focus on the degree of decline over a given period of capacity degradation to determine whether it is truly different from the inherent trend. The anomalous level of capacity degradation is then assessed as a key basis for subsequent tailored prediction strategies.

Fig. 4 shows a type of capacity degradation process for which there is an inherent trend. The orange arrows in Fig. 4 point in directions similar to the intrinsic trend. The red box shows a decline that is clearly different from the intrinsic trend. The green box shows a recovery following a decrease. This "V/U" shaped data segment, going down and then up, is the recoverable capacity proposed in this paper. Recoverable capacity has a short-term nature and recoverability compared to the long-term inherent trend of capacity degradation [30]. It is worth noting that short term anomalies, represented by recoverable capacity, can lead to fluctuations in prediction results, which in turn shorten prognostic horizons and reduce relative accuracy, as found in the previous study. Therefore, in this paper, we hope to extract the above data features for use in accurately identifying recoverable capacity, and to explore more reliable and trustworthy tailored prediction strategies based on them.

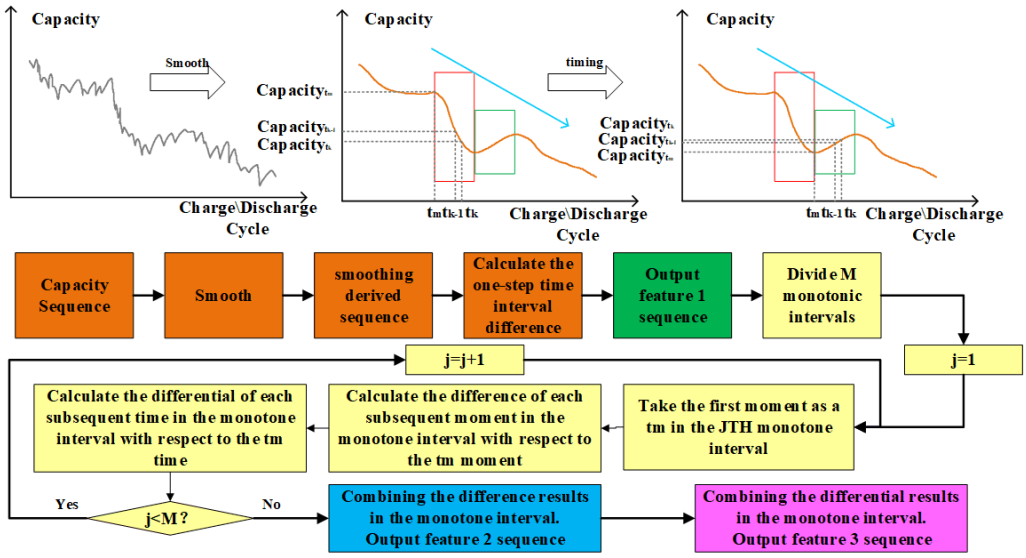

Fig. 4. Schematic diagram of recoverable capacity

When analyzing the difference between recoverable capacity and internal trends from the perspective of data, the most obvious difference is that recoverable capacity is characterized by rapid short-term changes. The recoverable capacity rapidly decreased by a certain order of magnitude in a short period of time, and then quickly increased by a certain order of magnitude, so the difference result was considered as the first feature ($F1$) to characterize this rapid change. For a known capacity series $Capacity_t (Capacity_t = [Capacity_{t_1}, Capacity_{t_2}, ..., Capacity_{t_k}])$, $F1$ is calculated according to the following formula.

$$F1_{t_k} = Capacity_{t_k} - Capacity_{t_{k-1}} \tag{4}$$

Where, t_k represents the time corresponding to the $k(k \in Z^*)$ sampling point, and $Capacity_{t_k}$ represents the health index at moment t_k.

$F1_{t_k}$ describes the change in $Capacity_{t_k}$ at moment t_k over $Capacity_{t_{k-1}}$ at moment t_{k-1}. According to $F1$, it can be determined whether the discharge capacity is in the decreasing stage, the increasing stage or the constant stage. This feature can also be used to find very large and very small values of the discharge capacity to determine whether the discharge capacity increases monotonically or decreases monotonically in a given time interval.

In addition, the two components of recoverable capacity, 'sag' and 'rise', are monotonic. This feature can be observed by calculating the change of continuous decrease or increase in a given monotonous interval. Therefore, the differential result in the monotone interval was considered as a second feature ($F2$) that characterizes the monotone feature.

$$F2_{t_k} = Capacity_{t_k} - Capacity_{t_m} \tag{5}$$

$F2_{t_k}$ describes the change in $Capacity_{t_k}$ at moment t_k over $Capacity_{t_m}$ at moment t_m, t_m is the previous extreme point at moment t_k. $F2$ can determine the amplitude of the discharge capacity change in the monotonous time interval. If the absolute value of $F2$ is very large over a very short time interval, it is likely to be a single data at that moment. If the absolute value of $F2$ increases over a long time interval, the discharge capacity is in the rising or falling stage at all time.

The rate of change of discharge capacity within the monotonic interval can reflect the speed of "sagging" and "rising", and can further determine the changes at different moments, so the differentiation results within the monotonic interval are considered as the third feature ($F3$) to characterize the amplitude change within this monotonic interval. $F3$ is calculated according to the following formula.

$$F3_{t_k} = \frac{Capacity_{t_k} - Capacity_{t_m}}{t_k - t_m} \tag{6}$$

The rate of change of the amplitude of the discharge capacity in a monotonous interval can be judged. If the absolute value of the discharge capacity increases and then decreases over a long time interval, the discharge capacity is in a stage of increasing and then rapidly decreasing and then slowly decreasing in the same time period.

All the above features are obtained through $Capacity_{t_1 \sim t_k}$, so they can all be calculated in real time during the actual operation.

In addition, during the degradation of Li-ion batteries, there are not only shorter periods of capacity degradation decline and recovery, as shown in Fig. 5. But there is also longer periods of inconsistent ability decline patterns, as shown in Fig. 6. Therefore, the change of actual production capacity alone may not meet the needs of determining the recoverable production capacity. Smoothing with different degradation capacity window lengths is necessary to obtain the total capacity degradation changes in the historical phase data.

Sliding window average [31] is a data processing method, which moves data with a fixed window size and calculates the average value of the data within each window. This method effectively smooths the data, reduces the influence of data fluctuations, and highlights trends and patterns in the data. And the computational complexity is relatively low. This enables real-time data to be processed quickly. A schematic of the short window smoothing is shown in Fig. 5 and a schematic of the long window smoothing is shown in Fig. 6.

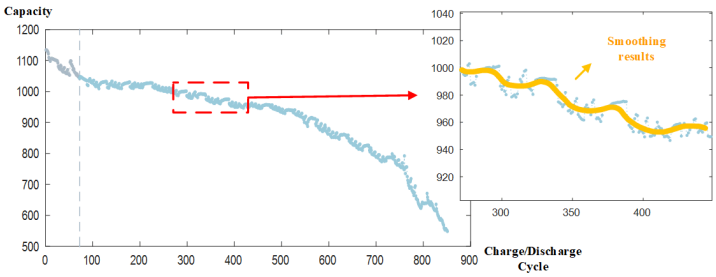

Fig. 5. Smoothing results with a short window

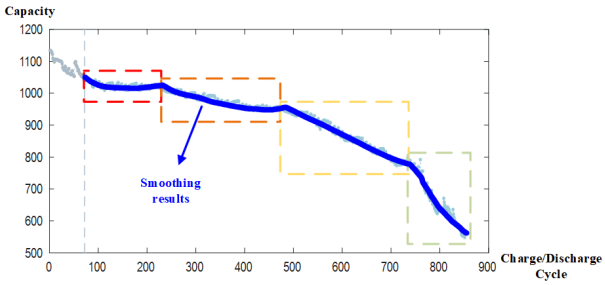

Fig. 6. Smoothing results with a long window

Smoothing based on short and long windows can result in two derived sequences of the target Li-ion battery historical data: a short window smoothed derived sequence ($Capacity_t^{short}$) and a long window smoothed derived sequence ($Capacity_t^{long}$). For these two derived sequences, the capacity degradation state detection based on "KS" was used to get different state labels of Li-ion battery when their capacity degrades, which provides a basis for the subsequent real-time evaluation of the degradation state.

Firstly, based on the constructed capacity degradation features $F1$, $F2$ and $F3$, the K- center clustering algorithm [32] is used to generate adaptive state labels of the discharge capacity ($Capacity$) degradation process. In order to better determine the number of categories of degraded states, the Gap Statistical Algorithm (GSA) [33] was used to find the best number of categories. It is roughly determined that the number of degradation status labels that may need to be generated is $K = 2,3,...,n$. According to different K values, the sum of squares of intra-class errors of the K-center clustering algorithm is calculated, and the K_{best} is determined by elbow criterion. Taking K_{best} as the target cluster number, and taking the capacity degradation features $F1$, $F2$ and $F3$ as input data, the corresponding $Label$ is obtained by K- center clustering algorithm.

Then, the Support Vector Machine (SVM) model [34] was trained, so as to obtain a state identification model of lithium-ion battery capacity deterioration that can be used for real-time state identification. Among them, the abnormal operation features $F1$, $F2$ and $F3$ are taken as inputs, and $Label$ obtained by the K-center clustering algorithm is taken as an output. It is expected that the degradation status labels obtained in this paper should clearly distinguish the internal trend from the recoverable capacity, and provide a more detailed representation of the different stages of the recoverable capacity. If $Label$ obtained based on the optimal number of clusters K_{best} is not able to distinguish clearly between recoverable capacity and inherent trend, a different value of K will be retried in order to obtain $Label$ capable of characterizing a different degradation state and to retrain the degradation state identification model.

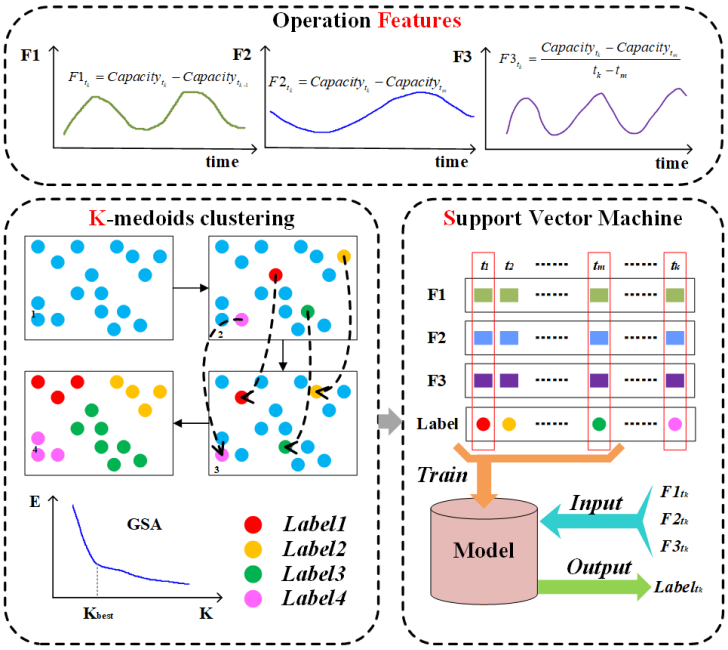

Fig. 7. Schematic diagram of the identification of the state of capacity degradation based on "KS".

2.3.2 A Prediction Strategy based on State Recognition and Adaptive Correction

From the long-term trend, the capacity of Li-ion batteries shows two states: decreasing and increasing. From the short-term trend, the capacity of Li-ion batteries shows three states: decreasing, stable and increasing. The prediction is achieved by adopting a correction strategy for two different states ($Label^{short}$ is the degradation state of the sequence derived from the short window and $Label^{long}$ is the degradation state of the sequence derived from the long window) that are at the same time. This prediction strategy is called State Recognition and Adaptive Correction (SRAC). The PKG estimated using this strategy is called SRAC-PKG. The LSTM trained using this strategy is called SRAC-LSTM. The PKG-LSTM obtained by this strategy is called SRAC-PKG-LSTM. As shown in Fig. 8.

Strategy 1: Assuming that $Label_{t_k}^{short}$ is stable in the time period $t_1 \sim t_k$, $Capacity_{t_1 \sim t_k}$ is used to estimate the bi-exponential model, the capacity degradation rate is extracted and grafted to $Capacity_{t_k}$ to obtain PKG. $Capacity_{t_1 \sim t_k}$ is used to train LSTM. PKG-LSTM is used to predict $Capacity_{t_{k+1}} \sim Capacity_{t_{k+n}}$. Record the time t_f corresponding to the capacity that reaches the threshold, and calculate $\widehat{RUL}_{t_i}$.

Strategy 2: Assuming that $Label_{t_k}^{short}$ is stable in the time period $t_1 \sim t_k$, $Capacity_{t_1 \sim t_k}$ is used to estimate the bi-exponential model, the capacity degradation rate is extracted and grafted to $Capacity_{t_k}$ to obtain PKG. If $Label_{t_k}^{long}$ is steady decreasing, $Capacity_{t_{k-p} \sim t_k}$ is corrected to $Capacity_{t_{k-p} \sim t_k}^{long}$. $[Capacity_{t_1 \sim t_{k-p}}, Capacity_{t_{k-p} \sim t_k}^{long}]$ is used to train LSTM. If $Label_{t_k}^{long}$ is rapid decreasing, $Capacity_{t_1 \sim t_{k-p}}$ is used to train LSTM. If $Label_{t_k}^{long}$ is increasing, $Capacity_{t_{k-p} \sim t_k}$ is corrected to $Capacity_{t_{k-p} \sim t_k}^{short}$. $[Capacity_{t_1 \sim t_{k-p}}, Capacity_{t_{k-p} \sim t_k}^{short}]$ is used to train LSTM. PKG-LSTM is used to predict $Capacity_{t_{k+1}} \sim Capacity_{t_{k+n}}$. Record the time t_f corresponding to the capacity that reaches the threshold, and calculate $\widehat{RUL}_{t_i}$.

Strategy 3: Assuming that $Label_{t_k}^{short}$ is increasing in the time period $t_1 \sim t_k$, $Capacity_{t_1 \sim t_k}$ is used to estimate the bi-exponential model, the capacity degradation rate is extracted and grafted to $Capacity_{t_k}$ to

obtain PKG. If $Label_{t_k}^{long}$ is steady decreasing or rapid decreasing, $Capacity_{t_{k-p}\sim t_k}$ is corrected to $Capacity_{t_{k-p}\sim t_k}^{long}$. $[Capacity_{t_1\sim t_{k-p}}, Capacity_{t_{k-p}\sim t_k}^{long}]$ is used to train LSTM. If $Label_{t_k}^{long}$ is increasing, $Capacity_{t_1\sim t_{k-p}}$ is used to train LSTM. PKG-LSTM is used to predict $Capacity_{t_{k+1}}\sim Capacity_{t_{k+n}}$. Record the time t_f corresponding to the capacity that reaches the threshold, and calculate $\widehat{RUL}_{t_i}$.

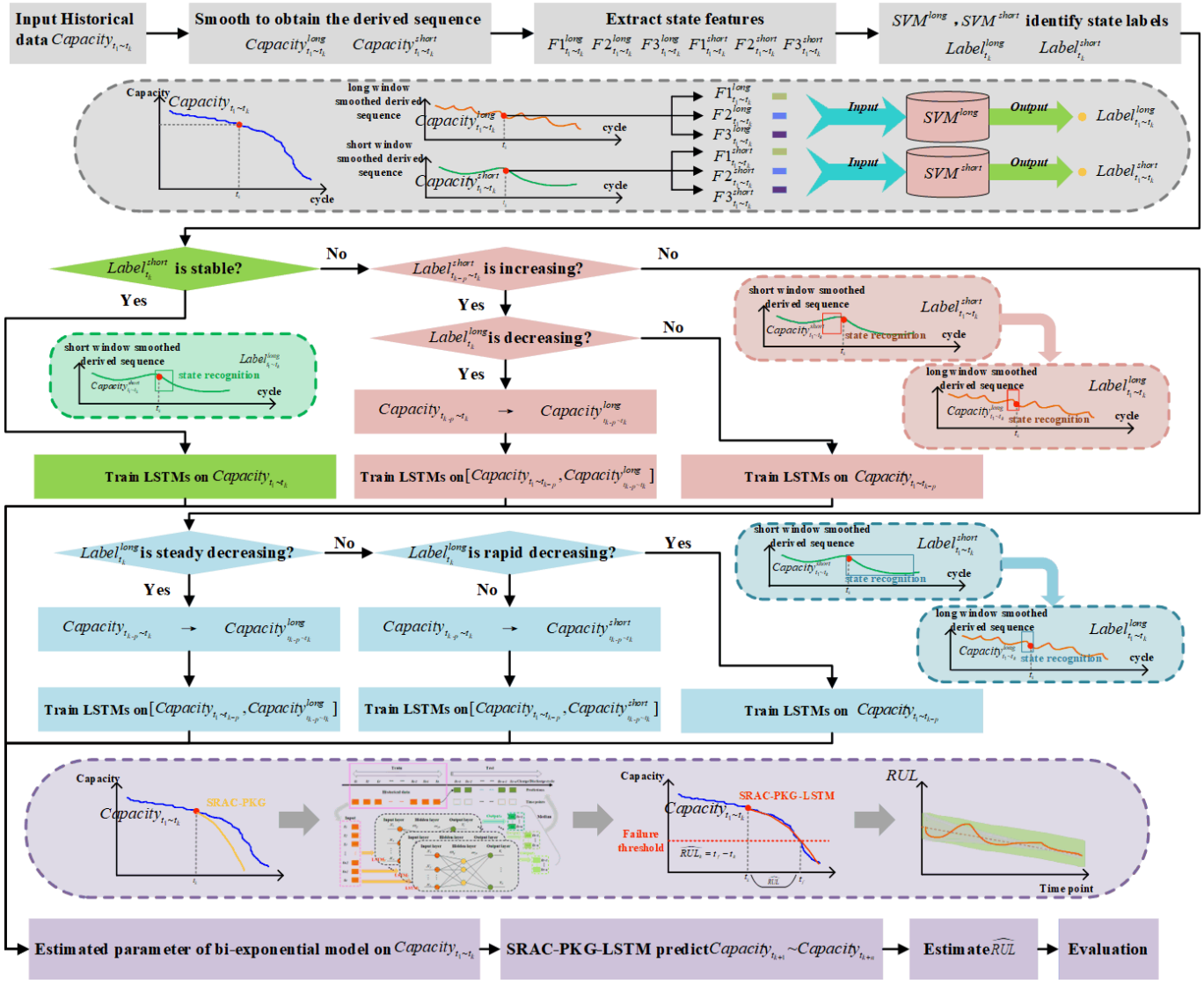

Fig. 8. Schematic diagram of the prediction strategy

3 Experiment

3.1 Dataset

Four Li-ion batteries, #35 #36 #37 #38 [35], of the CS2 model Li-ion battery from Center for Advanced Life Cycle Engineering (CALCE) Battery Research Group were used for the experiments. Where #35 #36 #38 were used as the reference Li-ion battery and #37 was used as the target Li-ion battery. Li-ion battery in the initial stage, its electrochemical performance is unstable, usually the actual charging and discharging capacity is higher than the rated capacity and capacity unstable degradation state. Therefore, data with a discharge capacity of 100% or more of the rated capacity was excluded and the RUL prediction was made from 100% capacity. It is necessary that estimating the parameters of the bi-exponential model and training the LSTM both require a certain amount of historical data. In this paper, at least 10% of the data from the previous period was used to estimate the model parameters and train the model.

3.2 Evaluation Metrics

(1) Evaluation Metrics for State Recognition

Accuracy is used to assess the number of correct model predictions as a proportion of the total sample size, the formula is as follows:

$$Accuracy = \frac{T}{T+F} \tag{7}$$

where T is the number of correct classifications in the sample total and F is the number of misclassifications in the sample total.

Precision to predict the results of the judgement based on the prediction for a particular category in the proportion of correct predictions, the formula is as follows:

$$Precision = \frac{TP}{TP+FP} \tag{8}$$

Where TP is the number of correct classifications in the prediction results and FP is the number of incorrect classifications in the prediction results.

Recall uses the actual sample as the basis for judgement and predicts as the proportion of predictions in a category, the formula is as follows:

$$Recall = \frac{TP}{TP+FN} \tag{9}$$

where FN is the number of cases of misclassification in the actual sample.

(2) Evaluation Metrics for Degradation Trend Prediction

In this paper, the assessment index of the degradation trend is MAPE [36], the formula is as follows:

$$MAPE = \frac{1}{n}\sum_{i=1}^{n}\left|\frac{\overline{y}_i - y_i}{y_i}\right| \times 100\% \tag{10}$$

(3) Evaluation Metrics for RUL Prediction

The remaining life assessment indices used in this paper are Relative Error (RE), Relative Accuracy (RA), Prognostic Horizon (PH) [37].

RE describes the error between the predicted result and the true result. For the remaining useful life, if RE is less than 0, it implies a conservative prediction, and if RE is greater than 0, it implies an aggressive prediction. The closer this value is to 0, the better, and the formula is as follows:

$$RE_{t_i} = \widehat{RUL}_{t_i} - RUL_{t_i} \tag{11}$$

A describes the percentage error of the prediction result at the current time, the higher the value the better, and is calculated as follows

$$RA_{t_i} = 1 - \left|\frac{\widehat{RUL}_{t_i} - RUL_{t_i}}{RUL_{t_i}}\right| \times 100\% \tag{12}$$

where RUL_{t_i} is the true remaining useful life at time t_i and $\widehat{RUL}_{t_i}$ is the RUL prediction of the model at time t_i. If $RA_{t_i} < 0$, then note RA_{t_i}=0.

The formula for PH at moment t_i is as follows:

$$\begin{cases} PH_{t_i} = EOL - t_{t_i}^{PH} \\ RUL_{t_i} - \alpha_{low} EOL \le CR_{t_i}^{PH} \le RUL_{t_i} + \alpha_{up} EOL \end{cases} \tag{13}$$

where EOL is the endpoint of the actual life, α_{low} and α_{up} are the lower and upper bounds of the

correction factor, and $CR_{t_i}^{PH}$ is the PH confidence interval for RUL_{t_i}.

4 Description and Analysis of Experiment Results

Starting from the 100th charge/discharge cycle, the experiment was conducted at a certain charge/discharge cycle interval. The sampling time points of the test are: 100, 134, 175, 215, 258, 301, 345, 388, 425, and 465. 50 LSTMs, PKG-LSTMs, SRAC-LSTMs and SRAC-PKG-LSTMs were trained for each sampling time point. The median predicted by 50 model is calculated as the final predicted battery capacity degradation trend. LSTM consists of 68 neurons in total, with 24 steps of input and 1 step of output.

4.1 Recoverable Capacity Identification

As shown in Figs. 9, the short window smoothed derived sequences and long window smoothed derived sequences, along with the corresponding degradation features, are presented for the reference Li-ion batteries #35, #36 and #38, and the target Li-ion battery #37, respectively. The length of the short window is 16 and the length of the long window is 50. The smoothed derived sequences were used to characterize the capacity degradation. The smoothing method is moving window average, so it can be used for real-time smoothing without using test data.

In Fig. 9, it can be observed that when $F1=0$, *Capacity* is usually at a certain extreme value. When $F1<0$, *Capacity* shows a decreasing trend. Conversely, when $F1>0$, *Capacity* shows an increasing trend. $F2$ is equally monotonic in the *Capacity* monotonic interval. In contrast to $F1$, which is relatively continuous and smooth overall, $F2$ shows some mutation points, indicating that the state has changed. For example, there is a transition from the descending state to an ascending state. $F3$ and $F2$ show similar characteristics, although $F2$ and $F3$ are different. $F3$ represents the property that *Capacity* contains time in monotonous interval. The three features of the data of these four Li-ion batteries show that all these Li-ion batteries show relatively obvious short-term fluctuations and can be recovered.

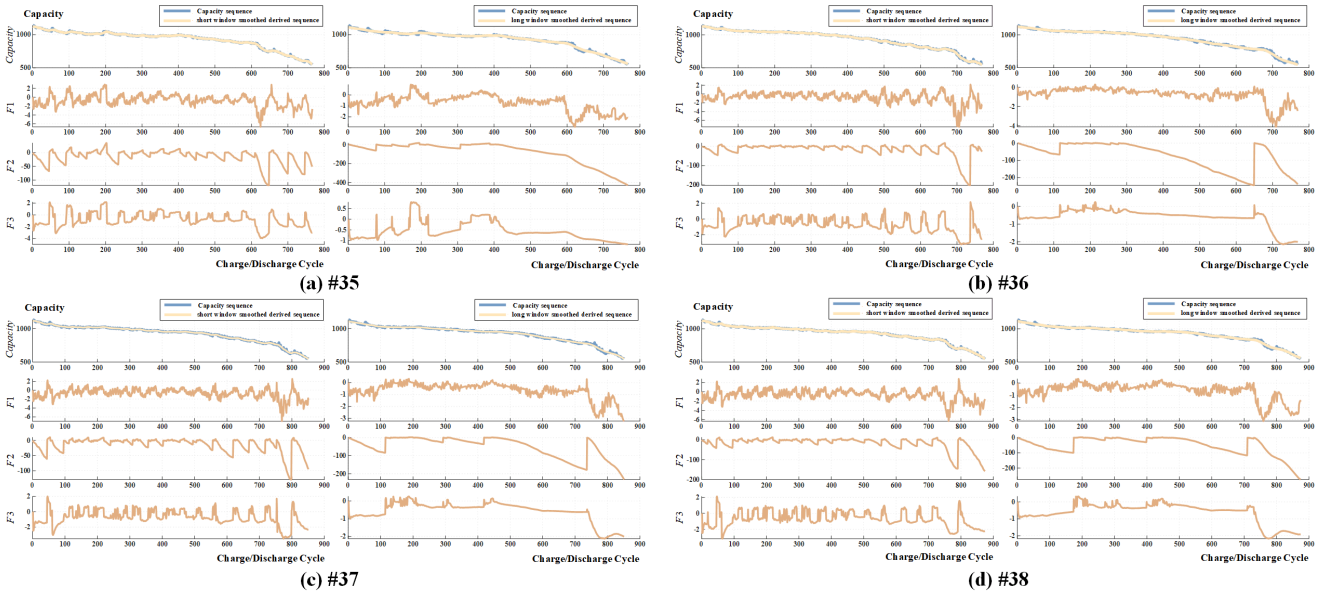

Fig. 9. Degradation features of Li-ion battery #35 #36 #37 #38

In order to determine the classification of degradation state of Li-ion batteries, $K=2,3,...,15$ is preset. The smooth short/long window derived sequences and corresponding degradation features of reference Li-ion batteries # 35, # 36 and # 38 are tested by K- center clustering algorithm. Fig. 10 shows the Cluster Sum of Square (CSS) for short window smoothing derived sequence degradation features for different values of *K*, the clustering results of the short window smoothing derived sequences on the feature space, and the degradation states during the reference Li-ion battery #35 #36 #38 decay process. It is evident that $K=4$ represents the most optimal clustering effect. In Fig. 10, it can be observed that of

the four categories, two have a clear downward trend, one has a clear upward trend, the remaining one is relatively stable, and the magnitude and rate of change of the two categories with a downward trend are somewhat different. The first state feature of capacity degradation in the short window is characterized by a small magnitude and rate of degradation, with an overall form of slow decay that is close to the intrinsic trend, which is later referred to as the Steady Stage. The second state feature is characterized by a larger magnitude and rate of degradation, with an overall rapid form of degradation that is clearly distinct from the intrinsic trend, which is later referred to as Descent Stage2. The third state feature is an intermediate state between the smooth and anomalous degradation states, with the magnitude and rate of degradation in between, and is the key state for determining recoverable capacity, which is later referred to as Descent Stage1. The fourth state feature is characterized by the Li-ion battery capacity being in an ascending state rather than a degradation state, which is later referred to as the Ascend Stage. It can be observed that Descent Stage1 and Descent Stage2 do not necessarily occur consecutively. Once Descent Stage2 has occurred, however, Ascend Stage is bound to follow. In light of the aforementioned findings, it is possible to make further refinements to the prediction strategy when it is being customized.

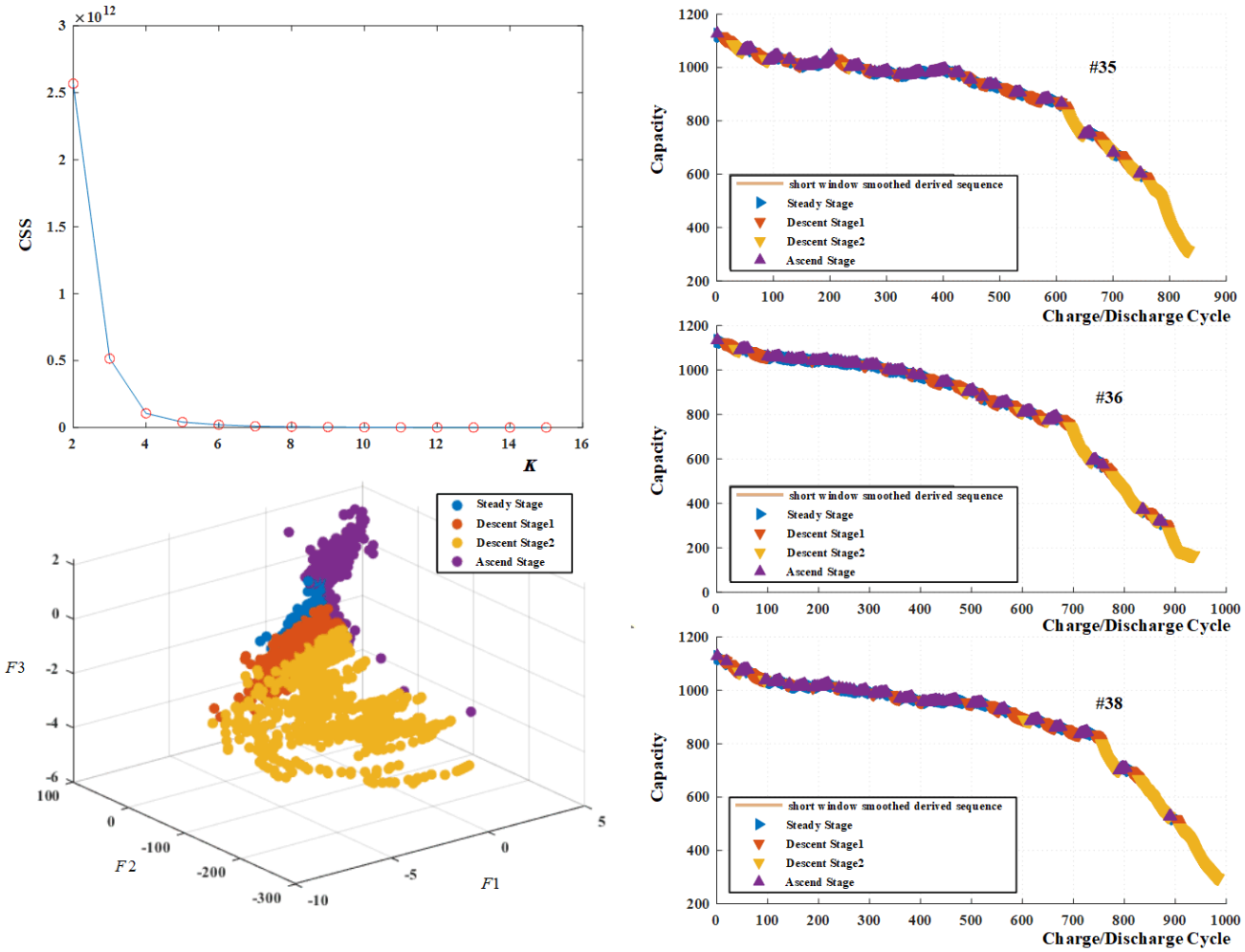

Fig. 10. Clustering results for #35 #36 #38 short window smoothing derived sequences

Fig. 11 illustrates the Cluster Sum of Square (CSS) for long window smoothing derived sequence decay features for different values of K, the clustering results of the short window smoothing derived sequences on the feature space, and the degradation states during the reference Li-ion battery #35 #36 #38 decay process. It is evident that $K = 3 or 4$ represents the most optimal clustering effect. In both cases $K = 3$ and $K = 4$, tests were conducted. A further category of clustering results was identified when $K = 4$, in comparison to the clustering results when $K = 3$. This additional category was found to be a stage subdivided from the second degradation period, as illustrated in Fig. 11. Although it is possible to

provide a more detailed representation of the degree of degradation, the additional class of degradation states is highly similar to the descending two-stage of the short window smoothed derived sequence and did not significantly contribute to the prediction strategy. The principle of streamlining and efficiency was upheld, resulting in the final selection of A=3. In Fig. 11, it can be observed that among these three categories, one is relatively stable, one has a clear downward trend, one has a clear upward trend. They are later referred to as the Descent Phase1, Descent Phase2 and Ascend Phase. The state clustering results from the reference Li-ion battery data were in accordance with the initial premise of this paper, which focuses on recoverable capacity. The data provided a detailed portrayal of the different phases of recoverable capacity, with the retention of a single phase to identify non-recoverable capacity.

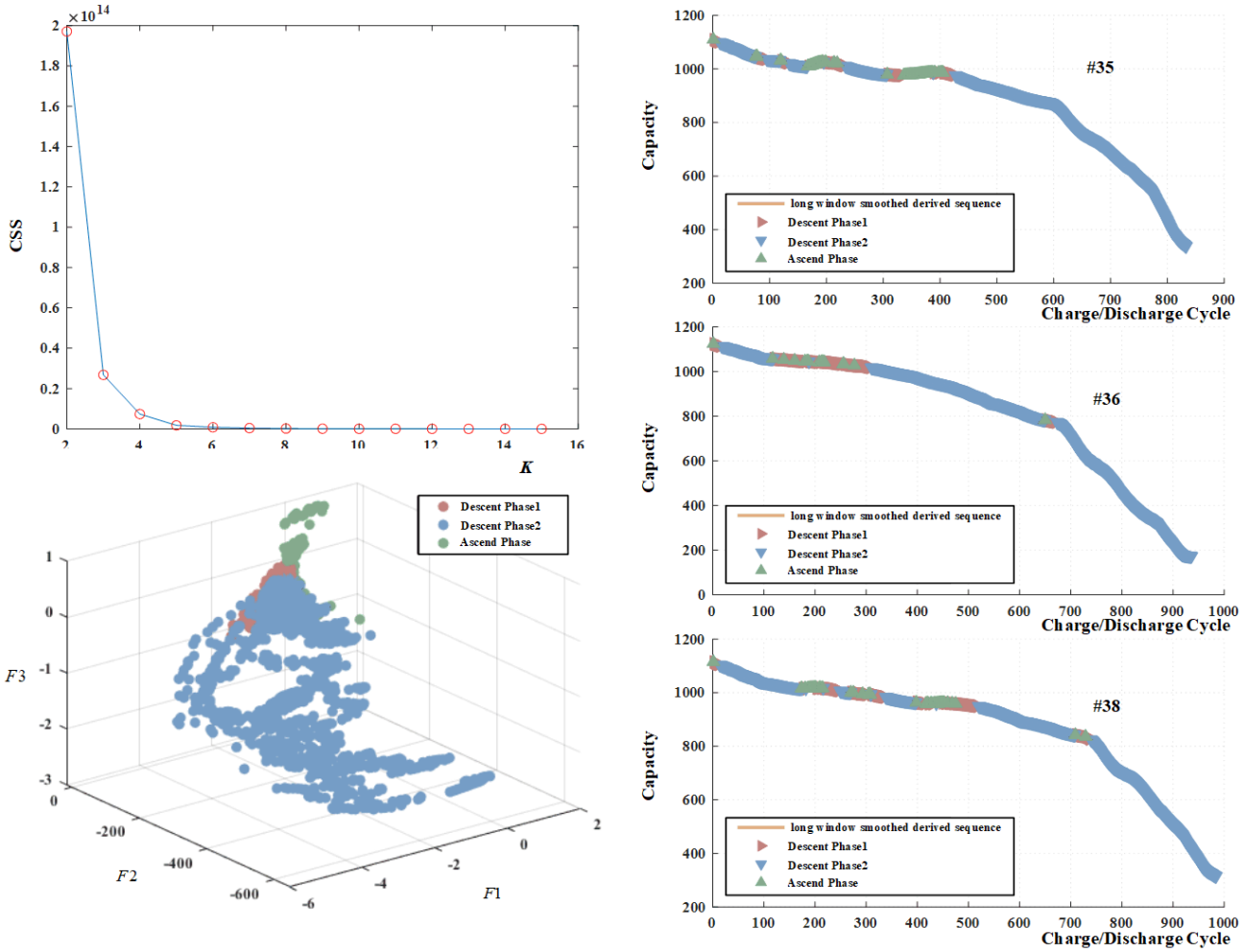

Fig. 11. Clustering results for #35 #36 #38 long window smoothing derived sequences

In order to obtain a solidified degradation battery state identification model for Li-ion batteries, the SVM model is chosen in this paper. The degradation state features corresponding to the short\long window smoothing derived sequences were used as inputs and the degradation state was used as outputs. Li-ion batteries #35 #36 #38 were used as training set and # 37 was used as test set. Fig. 12 illustrates the confusion matrix for the test results of the degradation state recognition model on the target Li-ion battery #37 short\long window smoothed derived sequence. The rows represent the true categories, and the corresponding prediction accuracy for the true aliases. The columns represent the predicted categories, and the corresponding prediction accuracy for the predicted categories. The accuracy of both was 95.18% and 97.41% respectively.

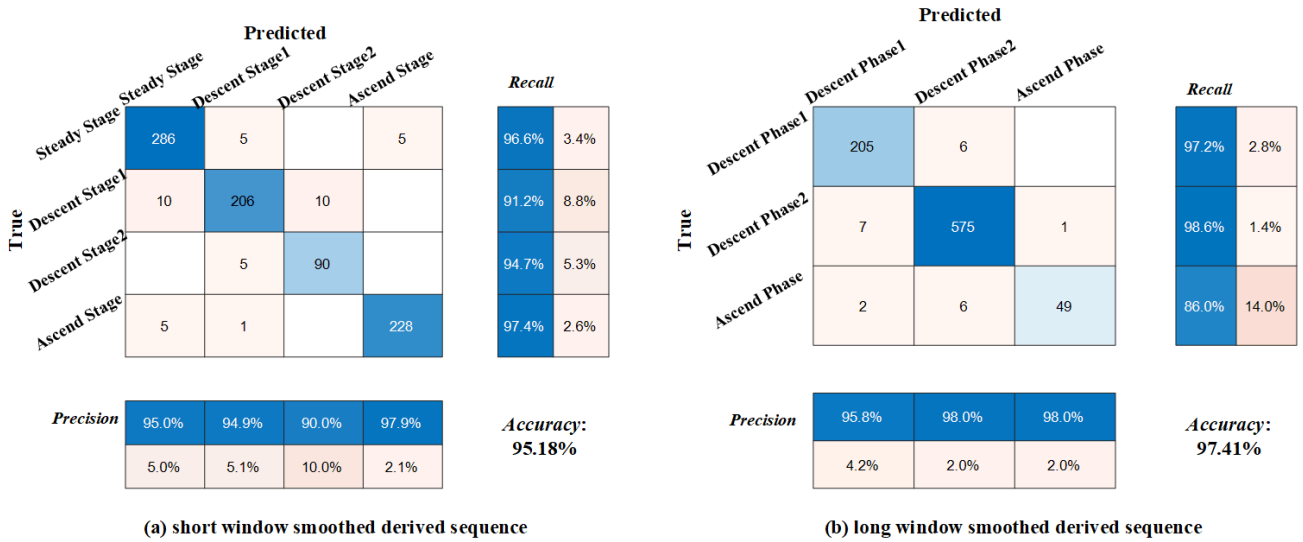

Fig. 12. Results of SVM model trained with reference to Li-ion battery #35 #36 #38 data

These two SVM models were subsequently used to identify the degradation state of the target Li-ion battery # 37 and both models were not re-trained during the subsequent ongoing expansion of the field of view. Fig. 13 illustrates two SVM models identifying the degradation state at each moment in the target Li-ion battery # 37. In Fig. 13, it can be observed that the degradation state of the long window smoothed derived sequence shows repeated fluctuations of "slight degradation-recovery" before reaching the first failure threshold of TF=880 (80% capacity), and then it shows a large degradation. The short window smoothed derived sequence degradation state shows frequent fluctuations of "degradation-recovery" until the third failure threshold TF=770 (70% capacity) is reached, after which a large degradation and a slight recovery are observed.

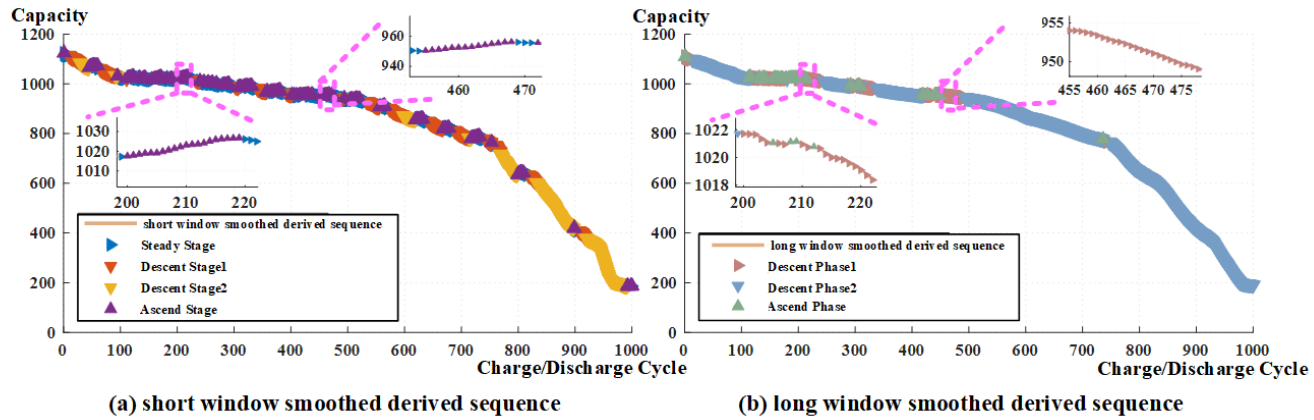

Fig. 13. Identification results of degradation state of Li-ion battery #37

4.2 Degradation Trend Prediction

Fig. 14 and Fig. 15 present some of the experiment results observed during the initial stages of Li-ion battery operation. Both figures display historical (train) data, future (test) data, a bi-exponential model with re-estimated parameters based on the target Li-ion battery, and the prediction trends of PKG, LSTM, and PKG-LSTM.

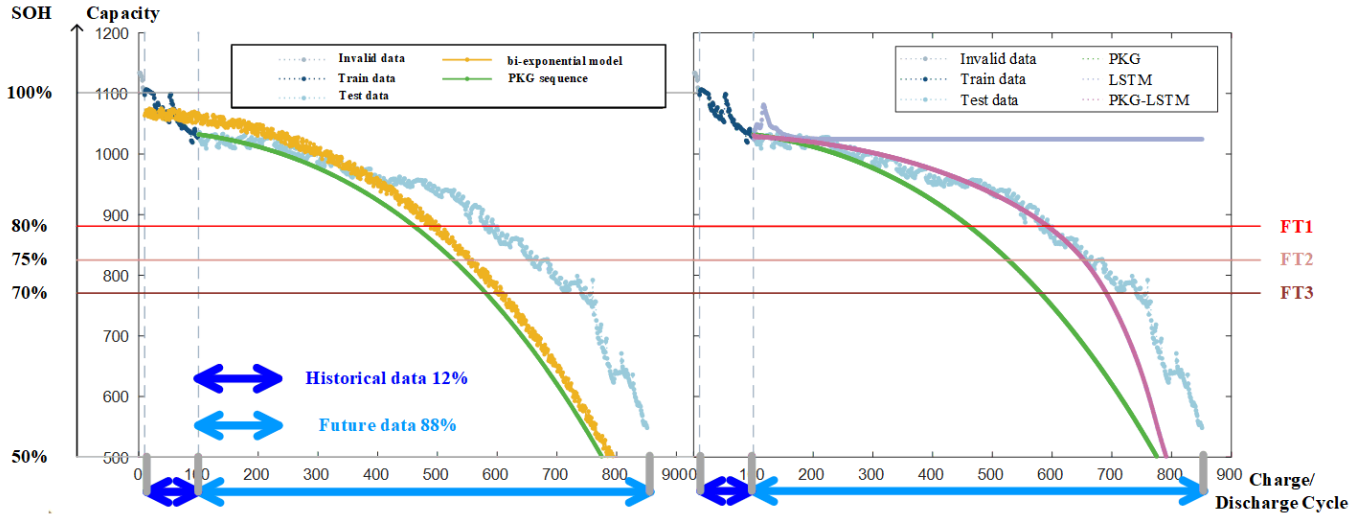

Fig. 14. PKG-LSTM predictions at the start of the 100th charge/discharge cycle

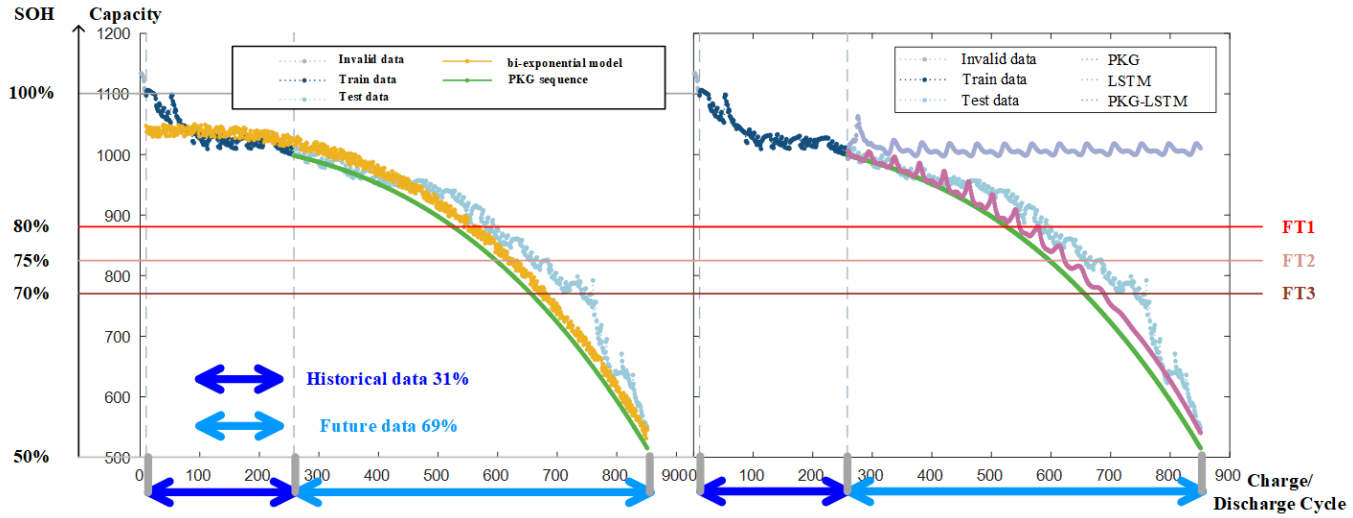

Fig. 15. PKG-LSTM predictions at the start of the 256th charge/discharge cycle

A total of five results out of ten sampling time points were modified with the implementation of the customized prediction strategy. These were the 134th, 215th, 345th, 425th, and 465th charge/discharge cycles. Fig. 16, Fig. 17, Fig. 18, Fig. 19 and Fig. 20 show the prediction results at the 134th, 215th, 345th, 425th, and 465th charge/discharge cycles of PKG-LSTM and SRAC-PKG-LSTM. Table 1 illustrates the evaluation metrics MAPE for the degradation trends of PKG-LSTM and SRAC-PKG-LSTM. The smaller these metrics, the smaller the overall prediction error, which implies a superior model.

In the experiments predicted at the 134th charge/discharge cycle, the degradation state at the 133rd and 134th charge/discharge cycles of the short window smoothing derived sequence was Ascend Stage, and the degradation state at the 134th charge/discharge cycle of the long window smoothing sequence was Descent Phase1, so the data of the 133rd and 134th charge/discharge cycles of the original capacity degradation sequence were corrected to be the data of the long window smoothing sequence of the 133rd and 134th charge/discharge cycle data of the long window smoothing sequence. In Fig. 16, it can be observed that the capacity degradation trend predicted by SRAC-PKG-LSTM is more in line with the inherent degradation trend of Li-ion batteries than that predicted by PKG-LSTM. From Table 1, it is found that the MAPE of SRAC-PKG-LSTM is 3.59% lower than that of PKG-LSTM.

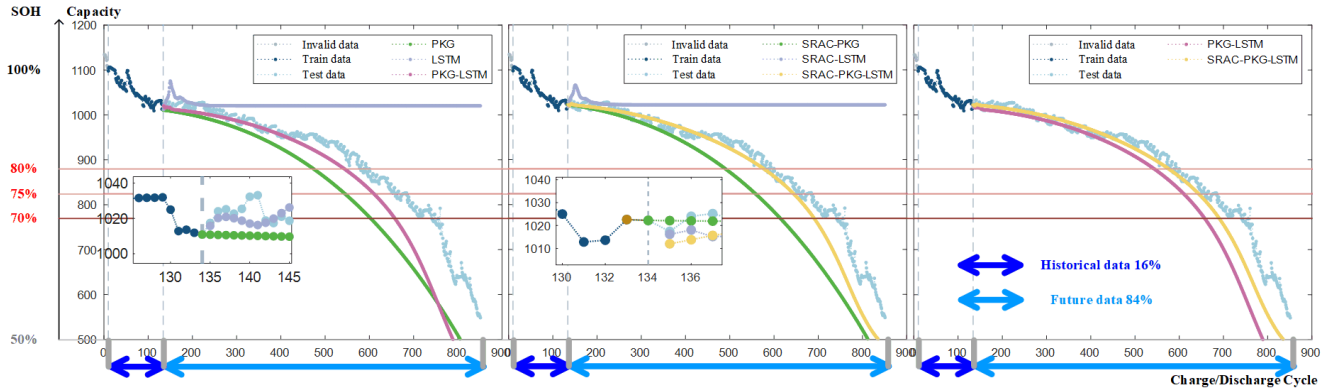

Fig. 16. PKG-LSTM vs SRAC-PKG-LSTM predictions at the 134th charge/discharge cycle

In the experiments predicted at the 215th charge/discharge cycle, the degradation state at the 200th to 215th charge/discharge cycles of the short window smoothing derived sequence was Ascend Stage, and the degradation state at the 215th charge/discharge cycle of the long window smoothing sequence was Descent Phase1. Therefore, the data of the 200th to 215th charge/discharge cycles of the original capacity decay sequence were corrected to the data of the 200th to 215th charge/discharge cycles of the long window smoothing sequence. In Fig. 17, it can be observed that the capacity degradation trend predicted by SRAC-PKG-LSTM is more in line with the inherent degradation trend of Li-ion batteries than the capacity degradation trend predicted by PKG-LSTM. From Table 1, it is found that the MAPE of SRAC-PKG-LSTM is 1.03% lower than that of PKG-LSTM.

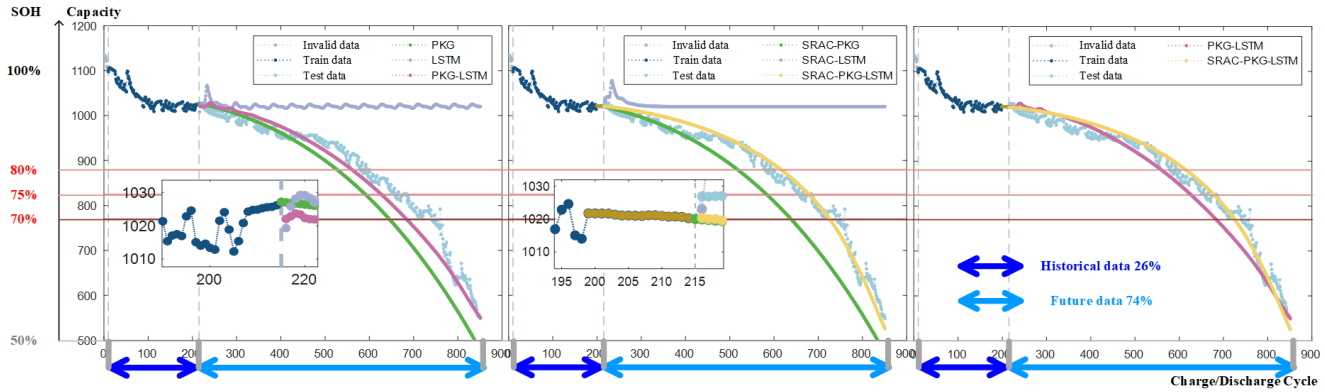

Fig. 17. PKG-LSTM vs SRAC-PKG-LSTM predictions at the 215th charge/discharge cycle

In the experiments predicted at the 345th charge/discharge cycle, the degradation state at the 341st to 345th charge/discharge cycles of the short window smoothing derived sequence was Descent Stage1, and the degradation state at the 345th charge/discharge cycle of the long window smoothing sequence was Descent Phase2. Therefore, the data of the 341st to 345th charge/discharge cycles of the original capacity decay sequence were corrected to the data of the 341st to 345th charge/discharge cycles of the long window smoothing sequence. In Fig. 18, it can be observed that the capacity degradation trend predicted by SRAC-PKG-LSTM has a small slowdown compared to the capacity degradation trend predicted by PKG-LSTM, and the overall trend is similar. From Table 1, it is found that the MAPE of SRAC-PKG-LSTM is 0.11% lower than that of PKG-LSTM.

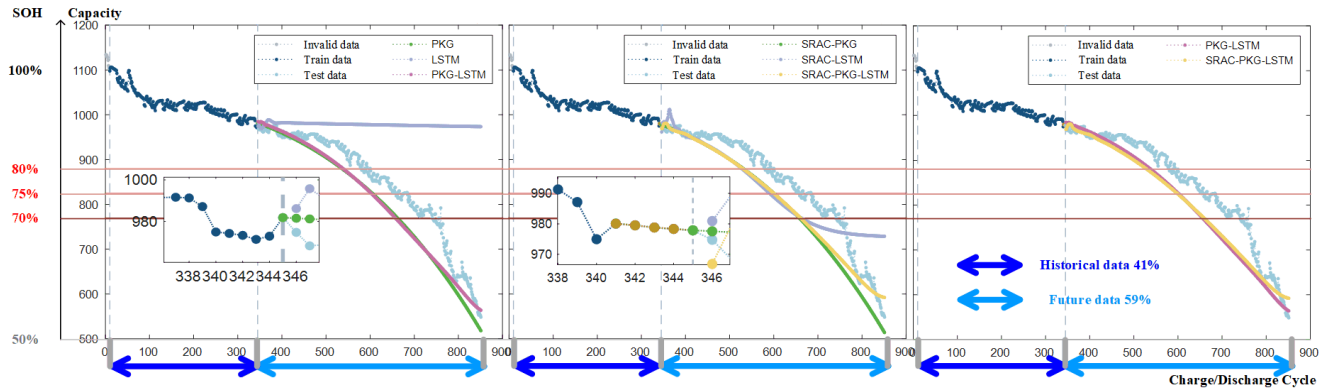

Fig. 18. PKG-LSTM vs SRAC-PKG-LSTM predictions at the 345th charge/discharge cycle

In the experiments predicted at the beginning of the 425th charge/discharge cycle, the degradation state at the 421st to 425th charge/discharge cycles of the short window smoothing derived sequence was Ascend Stage, and the degradation state at the 425th charge/discharge cycle of the long window smoothing sequence was Descent Phase1. Therefore, the data from the 421st to 425th charge/discharge cycles of the original capacity decay sequence were corrected to the data from the 421st to 425th charge/discharge cycles of the long window smoothing sequence. In Fig. 19, it can be observed that the capacity degradation trend predicted by SRAC-PKG-LSTM is more in line with the inherent degradation trend of Li-ion batteries than that predicted by PKG-LSTM. From Table 1, it is found that the MAPE of SRAC-PKG-LSTM is 0.36% lower than that of PKG-LSTM.

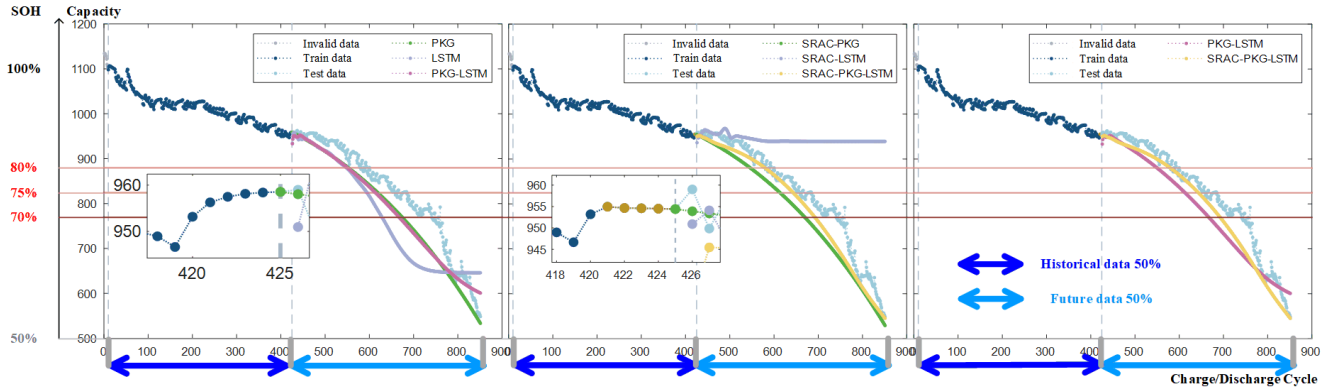

Fig. 19. PKG-LSTM vs SRAC-PKG-LSTM predictions at the 425th charge/discharge cycle

In the experiments predicted at the beginning of the 465th charge/discharge cycle, the degradation state at the 455th to 465th charge/discharge cycles of the short window smoothing derived sequence was Ascend Stage, and the degradation state at the 465th charge/discharge cycle of the long window smoothing sequence was Descent Phase1. Therefore, the data of the 455th to 465th charge/discharge cycles of the original capacity decay sequence were corrected to the data of the 455th to 465th charge/discharge cycles of the long window smoothing sequence. In Fig. 20, it can be observed that the capacity degradation trend predicted by SRAC-PKG-LSTM is more in line with the inherent degradation trend of Li-ion batteries than that predicted by PKG-LSTM. From Table 1, it is found that the MAPE of SRAC-PKG-LSTM is 1.12% lower than that of PKG-LSTM.

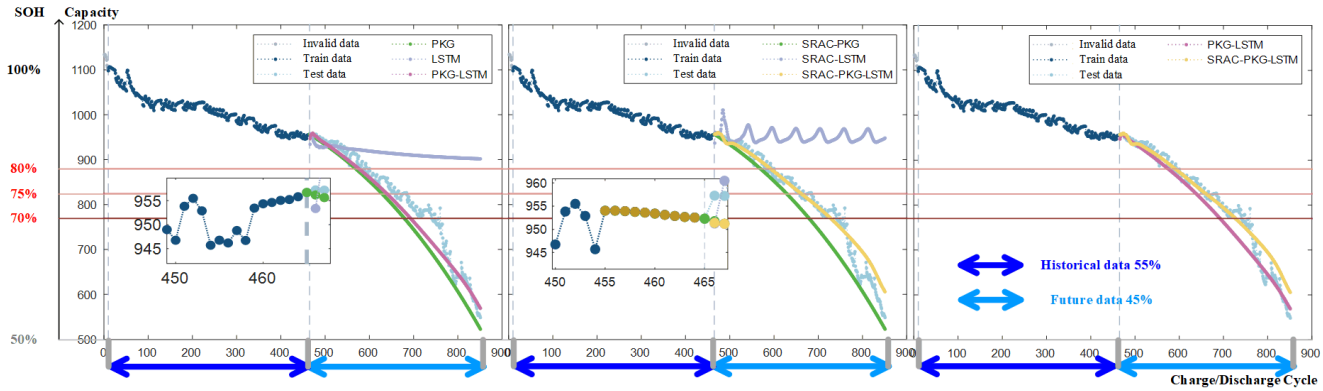

Fig. 20. PKG-LSTM vs SRAC-PKG-LSTM predictions at the 465th charge/discharge cycle

Table 1 MAPE for predicting degradation trends at different time points

Time point \ Model	PKG	SRAC-PKG	LSTM	SRAC-LSTM	PKG-LSTM	SRAC-PKG-LSTM
100	11.28%	11.28%	16.73%	16.73%	5.05%	**5.05%↓**
134	9.63%	9.36%	17.01%	17.20%	7.20%	**3.61%↓**
175	**2.62%↓**	**2.62%↓**	18.11%	18.11%	4.76%	4.76%
215	6.21%	6.72%	19.15%	19.19%	2.98%	**1.95%↓**
258	5.32%	5.32%	19.46%	19.46%	**2.52%↓**	**2.52%↓**
301	5.18%	5.18%	10.44%	10.44%	**4.16%↓**	**4.16%↓**
345	5.52%	5.93%	18.17%	6.39%	4.99%	**4.88%↓**
388	8.33%	8.33%	19.95%	19.95%	**4.73%↓**	**4.73%↓**
425	4.83%	4.74%	11.70%	10.10%	4.62%	**4.26%↓**
465	4.68%	4.57%	22.74%	21.81%	3.07%	**1.95%↓**

Table 2 Time cost(s) for predicting degradation trends at different time points

Time point		100	134	175	215	258	301	345	388	425	465	497
Model	PKG	6.4	7.9	6.59	6.63	6.68	5.15	6.19	7.57	6.49	9.9	7
	LSTM	60.46	68.51	75.41	80.44	92.13	95.95	107.51	122.58	130.79	147.25	137.92

As shown in Table 2 is time cost for predicting degradation trends at different time points, measured in seconds. The table shows the time it takes to generate PKG and the time it takes for a single LSTM. It is worth mentioning that the LSTM in the table represents the time spent by a single LSTM, not the integrated temporal network LSTMs. And the time shown includes the time of training using historical data and the time of predicting the future. The final model time consumption will be different according to the calculation method of the integrated temporal network. For example, in this paper, 50 LSTM of the integrated temporal network are divided into 10 groups, with 5 LSTM in each group. These 10 groups are calculated in series, and 5 LSTM in each group are calculated in parallel. It takes 10 times as long as the time in the table to the integrated temporal network LSTMs at a certain point in time.

At these test time points, SRAC-PKG-LSTM reduces MAPE by a maximum of 3.59% and an average of 1.24% compared to PKG-LSTM. As shown in Table 3 is the average MAPE of PKG-LSTM and RAC-PKG-LSTM on 10 test nodes. It can be found that SRAC-PKG-LSTM has a significant performance improvement with the customized strategy, and the MAPE has decreased from 4.41% to 3.79%. It is demonstrated that a prediction strategy based on adaptive correction of degradation states can effectively improve the ability of data-driven models to predict degradation trends.

Table 3 Comparison of MAPE metrics for degradation trend prediction

Model	LSTM	SRAC-LSTM	PKG-LSTM	CNN-LSTM [6]	CEEMD-LSTM [38]	SRAC-PKG-LSTM
MAPE	17.34%	15.94%	4.41%	5.28%	4.28%	**3.79%↓**

4.3 RUL Prediction

Fig. 21 and Table 4 show the RUL prediction results and evaluation indexes when the Li-ion battery failure threshold was set to eighty per cent of the rated capacity, i.e., TF = 880, when the true end-of-life was the 581st charge/discharge cycle. The upper and lower PH limits in Fig. 21 were set to 10 per cent, respectively. In the experiments, it was found that the prediction results in LSTM were often flat and tended to be constant, and even in most cases the RUL could not be estimated after predicting 5,000 charge/discharge cycling cycles, and therefore the prediction metrics of SRAC-LSTM could not be counted in Table 4. In order to have a significant comparison effect, in Fig. 21 the optimal prediction result of SRAC-LSTM was selected to plot it out, SRAC-PKG and SRAC-PKG-LSTM are plotted based on the actual output of the integrated model. In the RUL error plot, it can be observed that the results of SRAC-PKG are relatively conservative overall, and the estimated RULs are all earlier than the actual RULs, and most of them are below the PH. Most of the predicted results of SRAC-PKG-LSTM fall within the PH. Compared to PKG-LSTM, SRAC-PKG-LSTM has a smaller overall error. In Table 3, in the experiment results at the three nodes of 215th, 345th, and 425th charge/discharge cycles, the RA of SRAC-PKG is slightly lower than that of SRAC-PKG-LSTM, and in the rest of the nodes the RA of SRAC-PKG-LSTM is significantly higher than that of PKG.

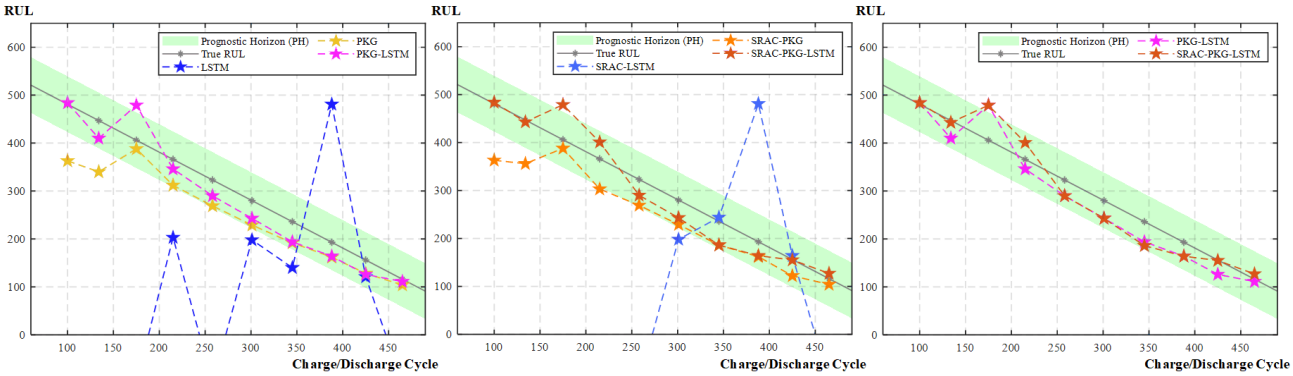

Fig. 21. TF=880 (80% Capacity), EOL=581, RUL error

Table 4 TF=880 (80% Capacity), EOL=581, RUL evaluation metrics

Node	RUL	PKG			LSTM			PKG-LSTM			SRAC-PKG-LSTM		
		$\widehat{RUL}$	*RE*	*RA*	$\widehat{RUL}$	*RE*	*RA*	$\widehat{RUL}$	*RE*	*RA*	$\widehat{RUL}$	*RE*	*RA*
100	481	363	-118	75.47%	-	-	0	484	**3**	**99.38%↑**	484	**3**	**99.38%↑**
134	447	340	-107	76.06%	-	-	0	410	**-37**	**91.72%↑**	443	**-4**	**99.11%↑**
175	406	388	**-18**	**95.57%↑**	-	-	0	479	73	82.02%	479	73	82.02%
215	366	312	-54	85.25%	-	-	0	346	**-20**	**94.54%↑**	401	35	90.44%
258	323	269	-54	83.28%	-	-	0	290	**-33**	**89.78%↑**	290	**-33**	**89.78%↑**
301	280	229	-51	81.79%	-	-	0	243	**-37**	**86.79%↑**	243	**-37**	**86.79%↑**
345	236	192	-44	81.36%	-	-	0	194	**-42**	**82.20%↑**	186	-50	78.81%
388	193	162	-31	83.94%	-	-	0	164	**-29**	**84.97%↑**	164	**-29**	**84.97%↑**
425	156	128	-28	82.05%	-	-	0	126	-30	80.77%	155	**-1**	**99.36%↑**
465	116	104	-12	89.66%	-	-	0	111	**-5**	**95.69%↑**	127	11	90.52%

Therefore, when eighty per cent of the rated capacity is the failure threshold, we conclude that the prediction result of SRAC-LSTM tends to be constant and cannot make a valid RUL prediction; the prediction result of SRAC-PKG is conservative and always gives premature RUL; and the prediction

result of SRAC-PKG-LSTM is basically in line with PH and slightly better than PKG-LSTM.

Fig. 22 and Table 5 demonstrate the RUL prediction results and evaluation metrics when the Li-ion battery failure threshold was set to seventy-five per cent of the rated capacity, i.e., TF = 825, when the true end-of-life time was the 659st charge/discharge cycle. The upper and lower limits of PH in Fig. 22 were set to 10 per cent, respectively. In the experiments, it was found that the prediction results in LSTM were often flat and tended to be constant, and even in most cases the RUL could not be estimated after predicting 5,000 charge/discharge cycling cycles, and therefore the prediction metrics of SRAC-LSTM could not be counted. In order to have a significant comparison effect, in Fig. 22 the optimal prediction result of SRAC-LSTM was selected to plot it out, SRAC-PKG and SRAC-PKG-LSTM are plotted based on the actual output of the integrated model. It can be observed in the RUL error plots that the SRAC-PKG results are overall more conservative, with the estimated RULs all earlier than the actual RULs, and most of them below the PH. The predictions of SRAC-PKG-LSTM all fall within the PH. Compared to PKG-LSTM, SRAC-PKG-LSTM has a smaller overall error and more results falling within the PH. In Table 5, in the experiment results at this node of the 345th charge/discharge cycle, the RA of SRAC-PKG is slightly lower than that of SRAC-PKG-LSTM, and the RA of SRAC-PKG-LSTM is significantly higher than that of PKG in the rest of the nodes.

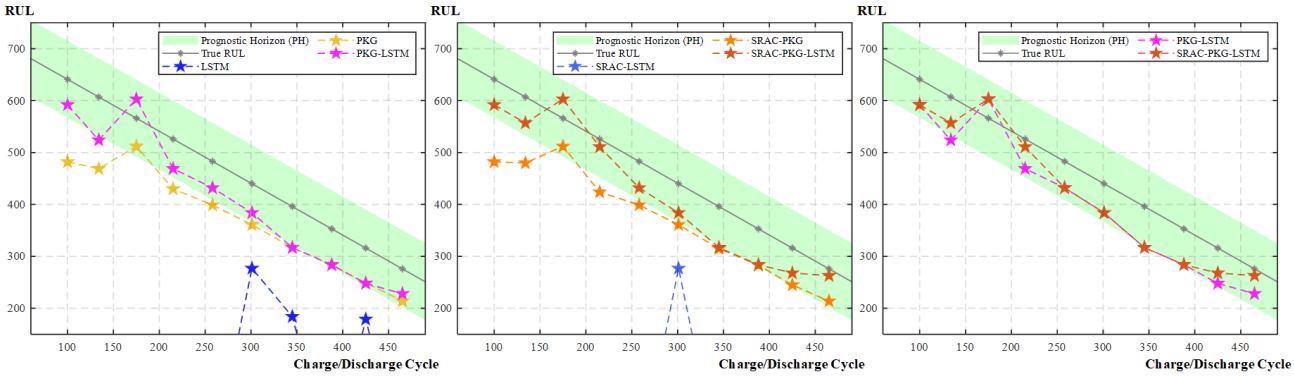

Fig. 22. TF=825 (75% Capacity), EOL=659, RUL error

Table 5 TF=825 (75% Capacity), EOL=659, RUL evaluation metrics

Node	RUL	PKG			LSTM			PKG-LSTM			SRAC-PKG-LSTM		
		$\widehat{RUL}$	*RE*	*RA*	$\widehat{RUL}$	*RE*	*RA*	$\widehat{RUL}$	*RE*	*RA*	$\widehat{RUL}$	*RE*	*RA*
100	481	427	-132	76.39%	-	-	0	554	**-5**	**99.11%↑**	554	**-5**	**99.11%↑**
134	447	411	-114	78.29%	-	-	0	476	-49	90.67%	510	**-15**	**97.14%↑**
175	406	455	**-29**	**94.01%↑**	-	-	0	549	65	86.57%	549	65	86.57%
215	366	376	-68	84.68%	-	-	0	412	-32	92.79%↑	464	**20**	**95.50%↑**
258	323	340	-61	84.79%	-	-	0	365	**-36**	**91.02%↑**	365	**-36**	**91.02%↑**
301	280	301	-57	84.08%	-	-	0	316	**-42**	**88.27%↑**	316	**-42**	**88.27%↑**
345	236	260	**-54**	**82.80%↑**	-	-	0	257	-57	81.85%	255	-59	81.21%
388	193	219	-52	80.81%	-	-	0	221	**-50**	**81.55%↑**	221	**-50**	**81.55%↑**
425	156	194	-40	82.91%	-	-	0	188	-46	80.34%	219	**-15**	**93.59%↑**
465	116	163	-31	84.02%	-	-	0	174	-20	89.69%↑	196	**2**	**98.97%↑**

Therefore, when seventy-five per cent of the rated capacity is the failure threshold, we conclude that: the prediction result of SRAC-LSTM tends to be constant and cannot make effective RUL prediction; the prediction result of SRAC-PKG is too conservative and always gives premature RUL; the prediction result of SRAC-PKG-LSTM is basically in line with PH, and it is better than that of PKG-LSTM.

Fig. 23 and Table 6 show the RUL prediction results and evaluation indexes when the failure threshold of Li-ion battery was set to seventy per cent of the rated capacity, i.e., TF=770, at which time

the true end-of-life time was the 741st charge/discharge cycle. The upper and lower limits of the PH and performance intervals in Fig. 23 were set to 10 per cent, respectively. In the experiments, it was found that the prediction results in LSTM were often flat and tended to be constant, and even in most cases the RUL could not be estimated after predicting 5,000 charge/discharge cycling cycles, and therefore the prediction metrics of SRAC-LSTM could not be counted. In order to have a significant comparison effect, in Fig. 23 the optimal prediction result of SRAC-LSTM was selected to plot it out, SRAC-PKG and SRAC-PKG-LSTM are plotted based on the actual output of the integrated model. It can be observed in the RUL error plots that the SRAC-PKG results are overall too conservative, with the estimated RULs all earlier than the actual RULs, and only very few results below the PH. The predictions of SRAC-PKG-LSTM all fall within the PH. Compared to PKG-LSTM, SRAC-PKG-LSTM has a smaller overall error. In Table 6, in the experiment results at this node of the 345th charge/discharge cycle, the RAs of SRAC-PKG and SRAC-PKG-LSTM are flat, and in the rest of the nodes the RAs of SRAC-PKG-LSTM are significantly higher than that of PKG.

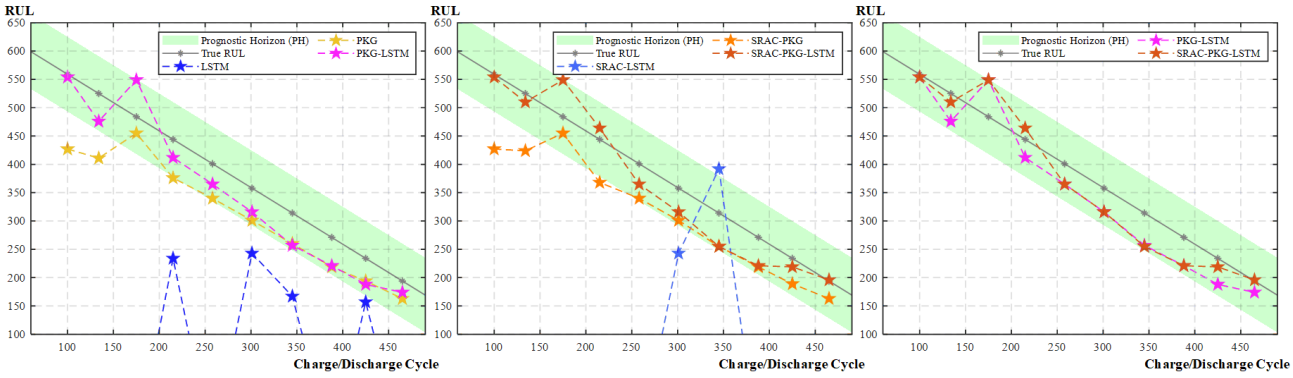

Fig. 23. TF=770 (70% Capacity), EOL=741, RUL error

Table 6 TF=770 (70% Capacity), EOL=741, RUL evaluation metrics

Node	RUL	PKG			LSTM			PKG-LSTM			SRAC-PKG-LSTM		
		$\widehat{RUL}$	*RE*	*RA*	$\widehat{RUL}$	*RE*	*RA*	$\widehat{RUL}$	*RE*	*RA*	$\widehat{RUL}$	*RE*	*RA*
100	481	482	-159	75.20%	-	-	0	592	**-49**	**92.36%↑**	592	**-49**	**92.36%↑**
134	447	469	-138	77.27%	-	-	0	524	-83	86.33%	557	**-50**	**91.76%↑**
175	406	512	-54	90.46%	-	-	0	603	**37**	**93.46%↑**	603	**37**	**93.46%↑**
215	366	430	-96	81.75%	-	-	0	469	-57	89.16%	511	**-15**	**97.15%↑**
258	323	399	-84	82.61%	-	-	0	432	**-51**	**89.44%↑**	432	**-51**	**89.44%↑**
301	280	361	-79	82.05%	-	-	0	384	**-56**	**87.27%↑**	384	**-56**	**87.27%↑**
345	236	317	**-79**	**80.05%↑**	-	-	0	312	**-84**	**80.05%↑**	317	**-79**	**80.05%↑**
388	193	283	-70	80.17%	-	-	0	284	**-69**	**80.45%↑**	284	**-69**	**80.45%↑**
425	156	249	-67	78.80%	-	-	0	243	-73	78.48%	268	**-48**	**84.81%↑**
465	116	214	-62	77.54%	-	-	0	228	-48	82.61%	263	**-13**	**95.29%↑**

Therefore, when seventy per cent of the rated capacity is the failure threshold, we conclude that: the prediction result of SRAC-LSTM tends to be constant and cannot make effective RUL prediction; the prediction result of SRAC-PKG is too conservative and always gives premature RUL; the prediction result of SRAC-PKG-LSTM is basically in line with PH, and it is better than PKG-LSTM.

Table 7 demonstrates the comparison of the remaining life prediction metrics for LSTM without customized prediction strategy, PKG-LSTM and SRAC-PKG-LSTM with customized prediction strategy at different failure thresholds. The metric used is the average value of RA on the 10 test nodes, which describes the overall prediction accuracy during the complete operation of the Li-ion battery. Since the LSTM does not estimate the RUL in most cases, it is not possible to calculate the average RA of the

LSTM. In Table 7, it can be found that with the addition of the customized prediction strategy, SRAC-PKG-LSTM has a significant improvement in the average RA over PKG-LSTM, with a maximum improvement of more than 3% and an average improvement of 2.56%. The experiments verify that the customized prediction strategy can effectively improve the prediction accuracy of PKG-LSTM, proving that the method proposed in this paper can effectively solve the unsatisfactory prediction accuracy caused by non-smooth trends.

Table 7 Average RA predicted by RUL for different failure thresholds

	TF=80% Capacity	TF=75% Capacity	TF=70% Capacity
LSTM	0	0	0
SRAC-LSTM	0	0	0
PKG-LSTM	88.79%	88.19%	85.94%
CNN-LSTM [6]	88.50%	89.12%	87.67%
CEEMD-LSTM [38]	83.46%	88.28%	79.98%
SRAC-PKG-LSTM	**90.12%↑**	**91.29%↑**	**89.18%↑**

Combining the above experiment results, LSTM and SRAC-LSTM are able to learn the characteristics of historical data, but the historical data are too small and inconsistent with the distribution characteristics of future data, and the degradation trend shows non-smoothness, which leads to the fact that LSTM and SRAC-LSTM are unable to fulfil the task of predicting the future change of Li-ion batteries' capacity, and therefore it is difficult to predict the RUL. PKG and SRAC-PKG are able to better portray the trend of Li-ion battery capacity degradation because of their own fixed mathematical form. PKG and SRAC-PKG show an overall trend of slower and then faster degradation. The slower degradation trend is more likely to be closer to the real degradation curve, but in the faster degradation part, PKG can't be adjusted according to the actual situation, which results in an overly conservative result. Thanks to the PKG that can provide the overall degradation trend of Li-ion batteries, the PKG-LSTM is able to express the capacity degradation features learnt in the historical data stage, and overall shows a better prediction capability. Thanks to the customized prediction strategy that is able to circumvent the historical end oscillation data, SRAC-PKG-LSTM improves the prediction capability by correcting part of the data of recoverable capacity, and obtains the prediction results that are more closely related to the actual degradation trend, as well as estimating RUL with smaller error, which is more stable and reliable overall.

5 Conclusion

In this paper, Empirical Model, Capacity Recovery-Identification Correction and Machine Learning co-driven method was proposed to solve the problem of RUL prediction for Li-ion batteries during real-world operation. Empirical formulae and data-driven are used to jointly complete the RUL predictions and address poor predictions caused by different data. Identify the recoverable capacity present during degradation and improve the prediction reliability of the model by correcting this data. The following conclusions can be summarized from the experiment results:

(1) The empirical model can better describe the overall trend of Li-ion battery degradation, although it can’t describe the details of the degradation, but it can provide a good reference for the machine learning model to help the model to better predict.

(2) Capacity recovery of Li-ion batteries can be identified.

(3) The overall prediction performance and reliability of the model can be improved by identifying recoverable capacity and correcting the data.

In future work, we will endeavor to explore the integration of additional physical degradation mechanisms into the identification and prediction of recoverable capacity. We will continue to advance the development of diagnostic-driven prediction models.

References

[1] Zio E. Some Challenges and Opportunities in Reliability Engineering. IEEE Transactions on Reliability.

2016;65(4):1769-1782. doi:10.1109/TR.2016.2591504

[2] Ding JF, Xu R, Yan C, Li BQ, Yuan H, Huang JQ. A review on the failure and regulation of solid electrolyte interphase in lithium batteries. Journal of Energy Chemistry. 2021;59:306-319. doi:10.1016/j.jechem.2020.11.016

[3] Zio E. Prognostics and Health Management (PHM): Where are we and where do we (need to) go in theory and practice. Reliability Engineering & System Safety. 2022;218:108119. doi:10.1016/j.ress.2021.108119

[4] Xia F, Tang C, Chen J. Online two-dimensional filter for anti-interference aging features extraction to accurately predict the battery health. Measurement. 2024;234:114758. doi:10.1016/j.measurement.2024.114758

[5] Xia F, Wang K, Chen J. State of health and remaining useful life prediction of lithium-ion batteries based on a disturbance-free incremental capacity and differential voltage analysis method. Journal of Energy Storage. 2023;64:107161. doi:10.1016/j.est.2023.107161

[6] Wang S, Jin S, Bai D, Fan Y, Shi H, Fernandez C. A critical review of improved deep learning methods for the remaining useful life prediction of lithium-ion batteries. Energy Reports. 2021;7:5562-5574. doi:10.1016/j.egyr.2021.08.182

[7] Xiao Y, Wen J, Yao L, Zheng J, Fang Z, Shen Y. A comprehensive review of the lithium-ion battery state of health prognosis methods combining aging mechanism analysis. Journal of Energy Storage. 2023;65:107347. doi:10.1016/j.est.2023.107347

[8] Li H, Zhang Z, Li T, Si X. A review on physics-informed data-driven remaining useful life prediction: Challenges and opportunities. Mechanical Systems and Signal Processing. 2024;209:111120. doi:10.1016/j.ymssp.2024.111120

[9] Hu X, Xu L, Lin X, Pecht M. Battery Lifetime Prognostics. Joule. 2020;4(2):310-346. doi:10.1016/j.joule.2019.11.018

[10] Qin T, Zeng S, Guo J. Robust prognostics for state of health estimation of lithium-ion batteries based on an improved PSO–SVR model. Microelectronics Reliability. 2015;55(9-10):1280-1284. doi:10.1016/j.microrel.2015.06.133

[11] Wang D, Miao Q, Pecht M. Prognostics of lithium-ion batteries based on relevance vectors and a conditional three-parameter capacity degradation model. Journal of Power Sources. 2013;239:253-264. doi:10.1016/j.jpowsour.2013.03.129

[12] Lin HT, Liang TJ, Chen SM. Estimation of Battery State of Health Using Probabilistic Neural Network. IEEE Trans Ind Inf. 2013;9(2):679-685. doi:10.1109/TII.2012.2222650

[13] He Z, Gao M, Ma G, Liu Y, Chen S. Online state-of-health estimation of lithium-ion batteries using Dynamic Bayesian Networks. Journal of Power Sources. 2014;267:576-583. doi:10.1016/j.jpowsour.2014.05.100

[14] Lee G, Kim J, Lee C. State-of-health estimation of Li-ion batteries in the early phases of qualification tests: An interpretable machine learning approach. Expert Systems with Applications. 2022;197:116817. doi:10.1016/j.eswa.2022.116817

[15] Lyu Z, Wang G, Gao R. Li-ion battery prognostic and health management through an indirect hybrid model. Journal of Energy Storage. 2021;42:102990. doi:10.1016/j.est.2021.102990

[16] Han H, Xu H, Yuan Z, Shen Y. A new SOH prediction model for lithium-ion battery for electric vehicles. In: 2014 17th International Conference on Electrical Machines and Systems (ICEMS). IEEE; 2014:997-1002. doi:10.1109/ICEMS.2014.7013631

[17] Li Y, Li Y, Pei A, et al. Atomic structure of sensitive battery materials and interfaces revealed by cryo–electron microscopy. Science. 2017;358(6362):506-510. doi:10.1126/science.aam6014

[18] Xiong R, Ma S, Li H, Sun F, Li J. Toward a Safer Battery Management System: A Critical Review on Diagnosis and Prognosis of Battery Short Circuit. iScience. 2020;23(4):101010. doi:10.1016/j.isci.2020.101010

[19] Aggab T, Avila M, Vrignat P, Kratz F. Unifying Model-Based Prognosis With Learning-Based Time-Series Prediction Methods: Application to Li-Ion Battery. IEEE Systems Journal. 2021;15(4):5245-5254. doi:10.1109/JSYST.2021.3080125

[20] Jiang M, Danilov DL, Eichel R, Notten PHL. A Review of Degradation Mechanisms and Recent Achievements for Ni-Rich Cathode-Based Li-Ion Batteries. Advanced Energy Materials. 2021;11(48):2103005.

doi:10.1002/aenm.202103005

[21] Chou JH, Wang FK, Lo SC. Predicting future capacity of lithium-ion batteries using transfer learning method. Journal of Energy Storage. 2023;71:108120. doi:10.1016/j.est.2023.108120

[22] Zhang Q, Tian Z, Niu J, Zhu J, Lu Y. A study on transfer learning in enhancing performance of building energy system fault diagnosis with extremely limited labeled data. Building and Environment. 2022;225:109641. doi:10.1016/j.buildenv.2022.109641

[23] Wang C, Li Z, Outbib R, Dou M, Zhao D. A novel long short-term memory networks-based data-driven prognostic strategy for proton exchange membrane fuel cells. International Journal of Hydrogen Energy. 2022;47(18):10395-10408. doi:10.1016/j.ijhydene.2022.01.121

[24] Li H, Fu L, Zhang Y. A novel hybrid data-driven method based on uncertainty quantification to predict the remaining useful life of lithium battery. Journal of Energy Storage. 2022;52:104984. doi:10.1016/j.est.2022.104984

[25] Yue M, Zhang X, Teng T, Meng J, Pahon E. Recursive performance prediction of automotive fuel cell based on conditional time series forecasting with convolutional neural network. International Journal of Hydrogen Energy. 2024;56:248-258. doi:10.1016/j.ijhydene.2023.12.168

[26] Wang T, Zhou H, Zhu C. A Short-Term and Long-Term Prognostic Method for PEM Fuel Cells Based on Gaussian Process Regression. Energies. 2022;15(13):4844. doi:10.3390/en15134844

[27] Zhang Y, Xiong R, He H, Pecht MG. Long Short-Term Memory Recurrent Neural Network for Remaining Useful Life Prediction of Lithium-Ion Batteries. IEEE Trans Veh Technol. 2018;67(7):5695-5705. doi:10.1109/TVT.2018.2805189

[28] Hou C, Han J, Liu P, et al. Operando Observations of SEI Film Evolution by Mass-Sensitive Scanning Transmission Electron Microscopy. Advanced Energy Materials. 2019;9(45):1902675. doi:10.1002/aenm.201902675

[29] Wang C, Li Z, Outbib R, Dou M, Zhao D. A novel long short-term memory networks-based data-driven prognostic strategy for proton exchange membrane fuel cells. International Journal of Hydrogen Energy. 2022;47(18):10395-10408. doi:10.1016/j.ijhydene.2022.01.121

[30] Berecibar M, Gandiaga I, Villarreal I, Omar N, Van Mierlo J, Van Den Bossche P. Critical review of state of health estimation methods of Li-ion batteries for real applications. Renewable and Sustainable Energy Reviews. 2016;56:572-587. doi:10.1016/j.rser.2015.11.042

[31] Lee C, Ryu T, Kim H, et al. Efficient approach of sliding window-based high average-utility pattern mining with list structures. Knowledge-Based Systems. 2022;256:109702. doi:10.1016/j.knosys.2022.109702

[32] Uribe-Hurtado AL, Orozco-Alzate M, Lopes N, Ribeiro B. GPU-based fast clustering via K-Centres and k-NN mode seeking for geospatial industry applications. Computers in Industry. 2020;122:103260. doi:10.1016/j.compind.2020.103260

[33] Zhang Y. Estimating the Number of Cluster in a Dataset via the Gap Statistic. University of Regina. 2006

[34] Lai Z, Liang G, Zhou J, Kong H, Lu Y. A joint learning framework for optimal feature extraction and multi-class SVM. Information Sciences. 2024;671:120656. doi:10.1016/j.ins.2024.120656

[35] Liu J, Liu X. An improved method of state of health prediction for lithium batteries considering different temperature. Journal of Energy Storage. 2023;63:107028. doi:10.1016/j.est.2023.107028

[36] Chen Z, Lv Z, Di R, et al. A novel virtual sample generation method to improve the quality of data and the accuracy of data-driven models. Neurocomputing. 2023;548:126380. doi:10.1016/j.neucom.2023.126380

[37] Wang C, Dou M, Li Z, et al. Data-driven prognostics based on time-frequency analysis and symbolic recurrent neural network for fuel cells under dynamic load. Reliability Engineering & System Safety. 2023;233:109123. doi:10.1016/j.ress.2023.109123

[38] Li H, Fu L, Zhang Y. A novel hybrid data-driven method based on uncertainty quantification to predict the remaining useful life of lithium battery. Journal of Energy Storage. 2022;52:104984. doi:10.1016/j.est.2022.104984